

Contents

1. Introduction	3
2. Theoretical Considerations	4
2.1. Positronium	4
2.2. Zeeman effect	5
2.3. Interaction of electromagnetic radiation with matter	6
2.4. Scintillators and photomultiplier tubes	7
2.5. Background coincidences	9
3. Setup and Conduction of the Experiment	10
3.1. Setup	10
3.2. Conduction	12
4. Analysis	13
4.1. Delay setup	13
4.2. ^{22}Na spectrum	13
4.3. 2γ -coincidences	15
4.3.1. Random coincidences	15
4.3.2. Angular dependence	16
4.3.3. Pressure dependence	18
4.4. 3γ -coincidences	20
4.4.1. Energy spectrum	20
4.4.2. Random coincidences	22
4.4.3. Hyper fine splitting	23
5. Summary and Discussion	25
Appendix	28
A. Error propagation	28
B. Additional Plots	28
C. Additional Tables	30
D. List of Figures	31
E. List of Tables	31
F. References	31
G. Acknowledgements	32
H. Laboratory Journal	32

1. Introduction

Positronium is the bound state of an electron and a positron [1]. After its existence had been proposed in 1932 by C. Anderson and S. Mohorovičić [3], the first experimental evidence of positronium was found in 1951 by M. Deutsch [4]. Since electrons and positrons annihilate each other, such a system is not stable and decays after a short time into γ -rays. This radiation can be detected and allows to draw conclusions about which state the positronium was in. Positronium is especially useful for the proof of certain predictions and as an illustration of phenomena in quantum electrodynamics (see for example [5], [6] or [7]).

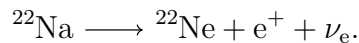
In this experiment the fine structure splitting of the ground state of positronium will be analyzed. For this an increasing magnetic field is applied, which leads to a reduction of the formation of the positronium state, which decays with an emission of 3 photons. This method is called quenching [8].

2. Theoretical Considerations

In this chapter the theoretical background of the experiment is depicted. The first section discusses what positronium is. The section after that describes the Zeeman effect and the final section in this chapter explains the method with which the random coincidence rates are determined.

2.1. Positronium

The quasi stable state called positronium consists of a bound electron e^- and positron e^+ [9]. In this experiment the positron is obtained from the β^+ decay of ^{22}Na to ^{22}Ne



When a positron is in close range to an electron they annihilate most of the time. If the energy of the positron lies in the Ore gap [10]

$$E_{\text{Ion}} - E_{\text{b}} < E_{e^+} < E_{\text{ex}},$$

together with an electron a positronium can be formed, a system similar to a hydrogen atom. Here the difference of the ionisation energy E_{Ion} of the electron and the binding energy of the positronium E_{b} is smaller than the energy of the positron E_{e^+} and the excitation energy of the electron source E_{ex} is larger. In this experiment the electron is taken from sulfur hexafluoride (SF_6) gas. Because of this the creation of more positronium is expected for a higher gas pressure. If the pressure is increased further, other effects, like Bremsstrahlung, shift the energy of the positron out of the Ore gap, reducing the formation of positronium.

Positronium can decay in different ways [1]. Which decay channel is taken depends on the total spin of the system in the ground state $L = 0$. If it is a triplet-state ($S=1$), where all spins are parallel, the system is called orthopositronium. The singlet-state ($S=0$) with anti-parallel spins is called parapositronium. A decay with only one γ -quant is not possible due to energy and momentum conservation. For para- and orthopositronium it is handy to look at the C -parity which describes the charge conjugation. n photons have a C -parity of $(-1)^n$ which has to be conserved. The C -parity of parapositronium is $C = +1$ as is shown in [11]. Thus parapositronium decays into an even number of photons. Orthopositronium on the other hand has $C = -1$, resulting in an odd number of photons. Figure 1 shows the two decays in their first order Feynmann graph. For parapositronium this is the decay channel with two and for orthopositronium with tree photons. Higher order decays have more vertices, which results in a reduced probability that this decay channel is taken and thus in a longer lifetime.

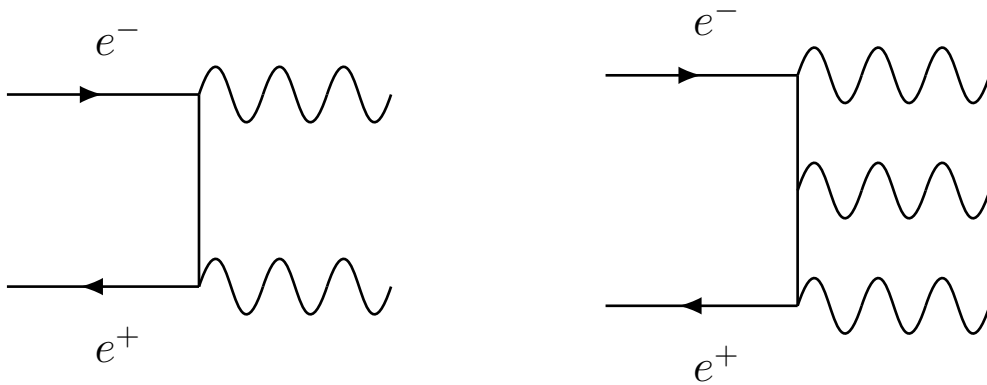


Fig. 1: First order Feynman diagrams of the decay of positronium into 2 (left) and 3 γ 's (right).

The total energy of positronium, which can be distributed between the photons, is two times the mass of an electron (1022 keV). In the 2γ -decay channel this energy is split evenly among the two photons with a lifetime of $\tau_{2\gamma} = 1.25 \cdot 10^{-10}$ s [10], which are emitted at an angle of 180° between each other. This is the result of momentum conservation in the rest frame of the positronium. The 3γ -decay channel has a lifetime of $\tau_{3\gamma} = 1.38 \cdot 10^{-7}$ s [10]. Here the energy is only split evenly between the three photons if they are emitted at an angle of 120° between each other. One photon can have a maximal possible energy of the mass of one electron (511 keV). In this case the other two photons have to move in the opposite direction to balance the momentum.

2.2. Zeeman effect

The Zeeman effect describes the splitting of spectral lines/energy levels by magnetic fields. Due to historical reasons one distinguishes between the normal and anomalous Zeeman effect. The normal effect describes systems, in which the electronic states have a net spin of zero. It describes the coupling of the orbit (l with magnetic number m_l) with a magnetic field. The anomalous effect describes systems for which the net spin is not equal to zero and is called that way, because at the time of the discovery the electron spin was not yet known. It describes the coupling of the spin and orbit to a magnetic field, where the coupling of l and s is weaker than the coupling to the magnetic field. If the field coupling is stronger, it is called Paschen-Back-effect [12]. Also in closed atomic shells, where no permanent magnetic moment is present, an external magnetic field induces a magnetic moment, which causes an extra splitting of the energy levels. In most atoms this so called quadratic Zeeman effect is substantially smaller compared to the linear effect.

However in the case of the positronium no linear effect is present and the quadratic effect is of leading order. This can easily be seen in the framework of perturbation theory. A derivation of this can be found in [1], where the time-independent Schrödinger equation is used. Using again the time-dependent Schrödinger equation, a magnetic field dependency of the formation of orthopositronium is found. The derivation is also shown in [1]. The ratio of para- and orthopositronium, also called quenching, which is dependent on the

magnetic field is

$$Q(B) = 1 - f + f \left(1 + \frac{\tau_{3\gamma}}{\tau_{2\gamma}} \left(\frac{e\hbar B}{m_e \Delta W} \right)^2 \right)^{-1}. \quad (1)$$

The factor f depends on the geometry of the setup. Since in this experiment the scintillators are set 120° apart, $f_{\text{theo}} = 0.5$ is expected, as stated in [8]. $\tau_{3\gamma} = 1.39 \cdot 10^{-7}$ s and $\tau_{2\gamma} = 1.25 \cdot 10^{-10}$ s are the lifetimes of ortho- and parapositronium [1]. e is the elementary charge, \hbar the reduced Planck constant, m_e the mass of an electron and ΔW the hyper fine splitting of the positronium ground state for a total spin of 0 and 1, with an expected value of $\Delta W_{\text{theo}} = 2.044 \cdot 10^5$ MHz [1].

2.3. Interaction of electromagnetic radiation with matter

There are three main processes, which are responsible for the interaction between electromagnetic radiation and matter [13]: the photoelectric effect, the Compton effect and pair production. The energy ranges in which they occur are shown in Figure 2.

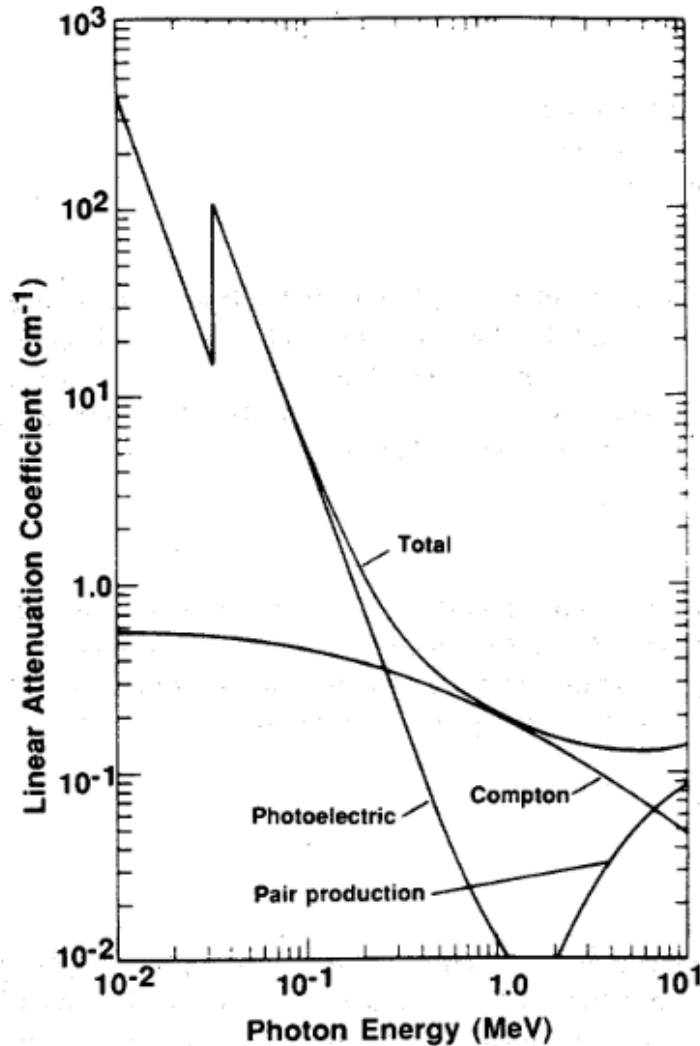


Fig. 2: Energy ranges of interaction processes of photons with matter taken from [14]. At low energies the photoelectric effect is dominant in the absorption process of photons. At larger energies the Compton effect gets more prominent until the pair production takes over.

Due to these interactions the intensity of the radiation decreases exponentially with a linearly increasing shielding thickness according to the Lambert-Beer law

$$I(d) = I(0) \exp(-\mu d).$$

d is the distance the radiation has traveled inside the matter, μ the absorption coefficient and $I(0)$ is the intensity of the incoming radiation.

Photoelectric Effect

In the photoelectric effect, which was first explained by Albert Einstein in 1905 [15], a photon transfers its total energy $E_\gamma = \hbar\omega$ to a shell electron. The energy of the excited electron is

$$E_e = E_\gamma - E_B,$$

with the binding energy E_B . If the energy of the photon is larger than the binding energy, the electron is expelled from its orbit. The resulting hole is filled by an electron from an outer shell under emission of a characteristic radiation or an Auger-Meitner electron.

Compton effect

The Compton effect describes the inelastic scattering of a photon with a free or weak bound electron [16]. The photon transfers a part of its energy to the electron which changes the movement directions of both photon and electron and thus also their energy.

Pair Production

Photons with at least two times the resting energy of an electron can lead to pair production, the creation of electron-positron pairs, in the field of a nucleus. This process only occurs for photons with energies larger than 1022 MeV, which is two times the resting mass of an electron or a positron (511 keV). Since positrons are meta-stable particles they annihilate again with an electron under the emission of at least two photons.

2.4. Scintillators and photomultiplier tubes

In this section the two core components of the setup used for detection of photons, the scintillator and the photomultiplier, are described in more detail.

A scintillator is a material, which exhibits scintillating properties, when irradiated with ionizing radiation. Incident photons excite the atoms of the scintillator which decay with the emission of lower energy photons. Those photons are then detected with a photomultiplier tube PMT (or a photodiode, or a silicon based photomultiplier SiPM) optically coupled to the scintillator. Since often the scintillator and the PMT have a different geometry (i.e., cross section area, circle or square) a light guide is needed to guide the photons onto the detection surface of the PMT. Once a photon hits the photocathode of the PMT electrons are emitted due to the photoeffect. The electrons are accelerated by a bias voltage towards the first dynode. When they hit the first dynode secondary electrons are emitted which again are accelerated towards the next dynode by an higher

bias voltage. This leads to an avalanche of electrons until the current is strong enough to be measured. This signal can then be related to the number of incident photons and their energy.

Scintillators are available in a variety of different shapes, materials and states of aggregation. They can be divided into organic or inorganic materials and gasses, liquids or solids. All show different characteristic behaviours in regard to their energy dependent resolution, linearity, time dependency, light yield, etc. The most common scintillators are NaI-crystals, which are also used in this experiment.

Obviously scintillators must be transparent to their own resonant photon-energies, which poses a technical difficulty. This problem can be solved by doping a different material into the crystals. In the case of NaI-crystals mostly thallium (TI) is used to activate the crystals. It introduces energy levels, which lie closely below the conduction band of the NaI-crystal and above the valence band. Excited atoms can decay onto those levels non-radiatively and then decay via emission of photons with an energy lower than the resonance energy of the NaI atoms. This doping can also be used to shift the energy of the scintillation photons into a frequency range, which coincides with the maximum sensitivity of the photomultiplier tubes. For most PMTs this is in the range of visible light, with a tendency to blue and ultraviolet.

There are many factors which have an influence on the statistics and resolutions. The energy resolution is directly proportional to the number of photons produced in the scintillator. The so called light yield L is defined as the number of photons emitted, when an incident particle loses a specific energy E in a certain length x of the crystal

$$\frac{dE}{dx} \propto \frac{dL}{dx}.$$

One would assume a Poisson distribution for this behaviour, which is mostly true. With this assumption it is easy to see, that materials that have a high light yield must have a high energy resolution. To reconstruct the energy of the incident particle correctly, the particle must lose all of its energy in the detection crystal. If that is the case, “the naive assumption of Poisson statistics is incorrect”[†], but it can be corrected for by introducing the Fano factor F . When the incident particle loses all of its energy in the crystal, the scintillation events are not independently of one another, since a definite amount of energy is deposited and not a fluctuating one, like in the case of a particle only passing through the detector. The Fano factor describes this behaviour. It is material dependent and can be experimentally determined. For NaI it is approximately 1. In general the energy dependent resolution R of a scintillator is calculated with

$$R = \frac{\Delta E}{E},$$

where ΔE , identified as the full width at half maximum of a peak is divided by its energy. With the relation between the FWHM of a Gaussian and its standard deviation σ and $J = E/w$, the number of ionizations, with E the deposited energy in the detector and w the mean energy required to ionize the material, the resolution results in

$$R = 2.35 \frac{\sqrt{FJ}}{J} = 2.35 \sqrt{\frac{Fw}{E}},$$

[†]Quote from William R. Leo in [17].

with the Fano factor F . In general a high light yield is wanted, since it increases the energy resolution of the detector. As described, the scintillator is optically coupled to a light guide, which has a collection and transmission efficiency, which feeds the photons into the PMT, which has a quantum efficiency. All this attributes to a loss in photons and therefore resolution.

2.5. Background coincidences

The background present in the 2 and 3 γ -coincidence measurements have numerous origins, but can be expressed as the random coincidences N_{random} . In the following, the derivation to obtain N_{random} for a 2 γ -coincidence is described. $N_{\text{random}, 3\gamma}$ is analogously derived.

In a coincidence measurement two or more signals have to coincide within a certain time window τ to be counted as a coincidence. While detector one (D1) opens a coincidence window of length τ , D2 will measure $\dot{N}_2 \tau$ events in average, where \dot{N}_2 is the average counting rate of D2 in the measurement time T . Together one already gets

$$N_{\text{random}, 2\gamma, 1} = N_1 \dot{N}_2 \tau = N_1 N_2 \frac{\tau}{T}$$

random coincidences. Of course this same process also happens if D2 opens a window, which results in an overall factor of 2 (for a 3 γ -coincidence a factor of 3)

$$N_{\text{random}, 2\gamma} = 2N_1 N_2 \frac{\tau}{T}, \quad \dot{N}_{\text{random}, 2\gamma} = 2\dot{N}_1 \dot{N}_2 \tau, \quad (2)$$

$$N_{\text{random}, 3\gamma} = 3N_1 N_2 N_3 \frac{\tau^2}{T^2}, \quad \dot{N}_{\text{random}, 3\gamma} = 3\dot{N}_1 \dot{N}_2 \dot{N}_3 \tau^2. \quad (3)$$

With these formulas and the known value of τ , random coincidence rates can be calculated.

3. Setup and Conduction of the Experiment

3.1. Setup

The main part of the used setup is shown in Figure 3. Figure 4 is another schematic picture of the setup, which focuses on the electronics and the signals pathways.

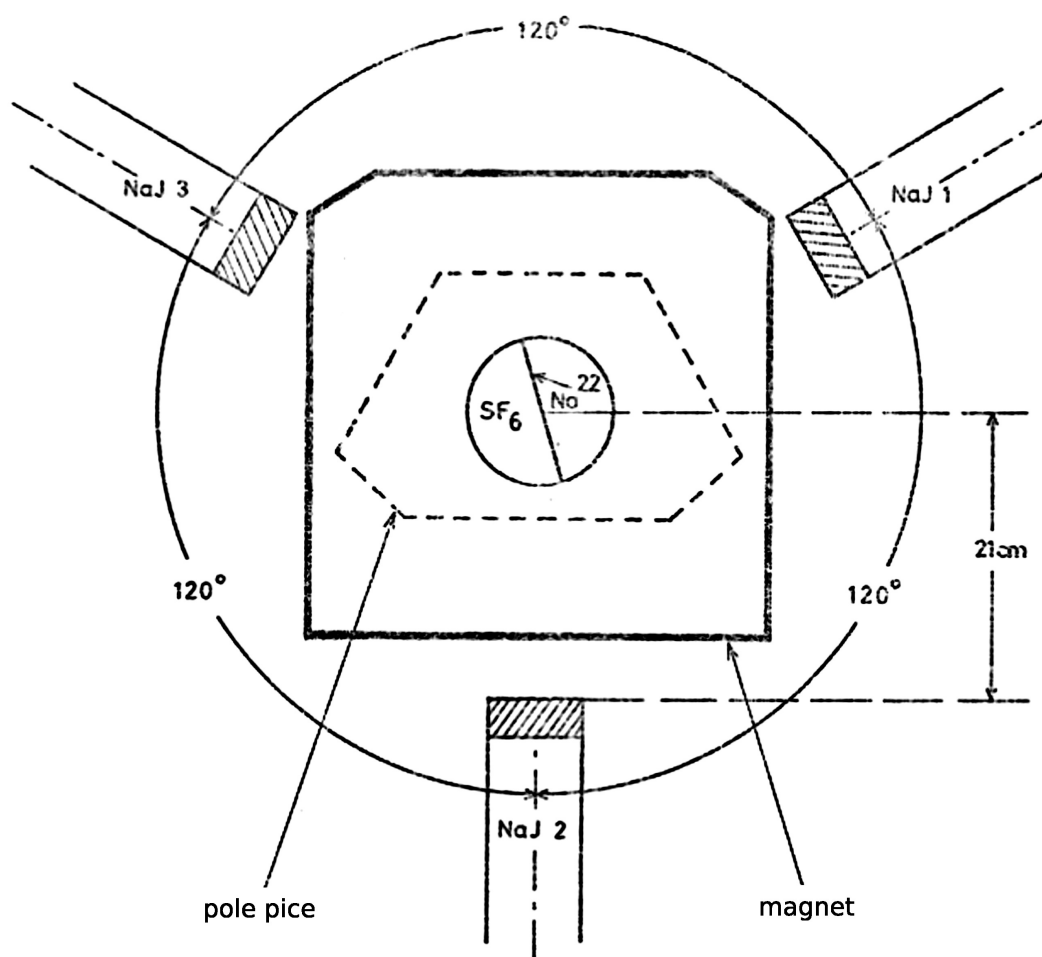


Fig. 3: Schematic picture of the core part of the setup, modified from [1]. Three NaI scintillators, labeled as NaJ, are shown in a 120° configuration. The scintillators 1 and 3 can be moved by approximately 180° . Scintillator 2 is fixed.

As positron source, ^{22}Na is used. It has a lifetime of 2.6a [1]. Since the source was build into the setup in 2004 it has to be hoped that enough radioactive material is still left for sufficiently high counting rates. The source is mounted on a plastic film which is positioned inside a box. This box is connected to a gas bottle of sulfur hexafluoride (SF_6), which acts as source for the electrons. The gas pressure provided by a gas bottle can be varied up to 7 bar with a pressure regulator valve (see Section 4.3.2).

The photons of the positronium decay are detected by three scintillator and photomultiplier units which are arranged in a circle, with adjustable polar positions around the source. Their working principle is explained in Section 2.4.

The angular position of scintillator 1 and 3 can be changed in a range of 90° to 270° compared to the fixed scintillator 2. The angles are read off of a scale which is fixed to the setup and might be inaccurately positioned. The electronic setup which is used for the detection and data acquisition is shown in Figure 4.

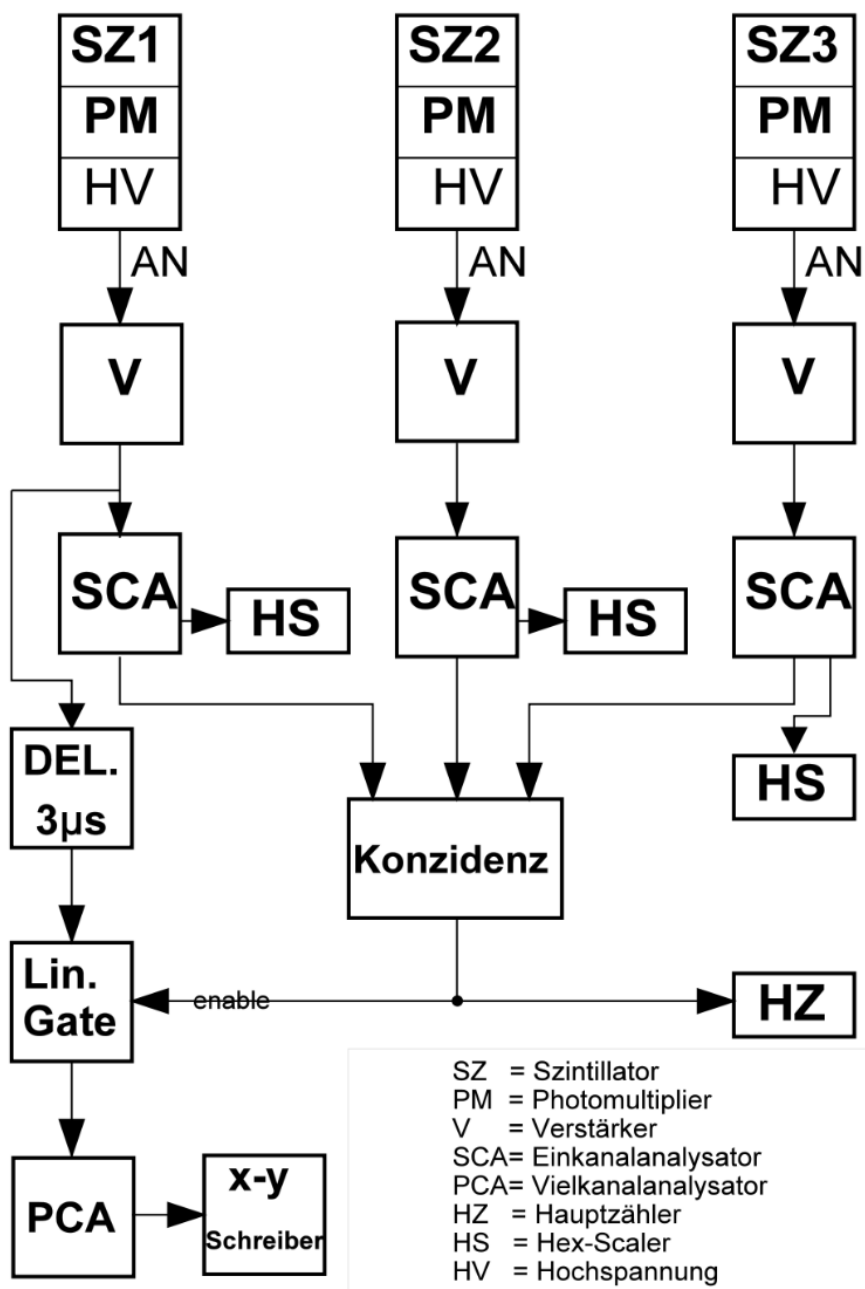


Fig. 4: Setup of the electronic components of the experiment. The photons are detected with the three scintillators (SZ1, SZ2, SZ3). PM are the photomultipliers and HV are the high voltage supplies, V the main amplifiers, SCA the single channel analyzers and HS the hex-scaler. HZ is the coincidence counter, PCA the multi channel analyzer (MCA) and the “x-y Schreiber” the PC, where software is used to read out the MCA. The figure is taken from [8].

The signals of the photomultipliers are amplified by the preamplifiers. The main amplifier shape and further amplify the signals. The single channel analyzers (SCA) are used to

discriminate signals by their corresponding incident photon energy. If such a signal is measured in a SCA, it sends out an logical yes, which is counted with the hex-scaler and also sent into a coincidence unit. The original signal is sent into a linear gate via a delay unit. This gate is opened by the coincidence unit. Up to three of the SCAs signals have to contribute, depending on the settings, in order for the coincidence unit to send a logical yes to the linear gate. The number of coincidences is also counted in the hex-scaler, while the signal which passes the linear gate is sent to a computer via a multi channel analyzer.

For measurements concerning the Zeeman effect a magnetic field is applied. For this an electromagnet surrounds the central box perpendicular. Its current is controlled with a power supply.

3.2. Conduction

This experiment is divided into two main parts: In the first part the setup is analyzed and in the second the quenching of the 3γ decay is studied.

The first measurement takes a closer look at the used electronics and how they influence the incoming signals. For this the outputs of the SCAs are connected to an oscilloscope. Then the source is analyzed by taking the ^{22}Na spectrum with all three scintillators individually. These measurements allow energy calibrations of the MCA for all scintillators. The angle correlation of the 2γ coincidences is studied by moving scintillator 1 between the 160° and 230° marks and measuring the coincidences with scintillator 2. Scintillator 3 is randomly set to 260° . In order to determine the random coincidences the signal of scintillator 2 is delayed heavily, such that a coincidence with scintillator 1 cannot result from the same 2γ decay. In the last measurement with the 2γ dependence the pressure of the SF_6 is changed in order to find the pressure, which yields the highest coincidence rate.

For the 3γ measurements the scintillators are positioned 120° apart from each other. With this setup the random coincidences are determined, as now the boundary condition has changed to a 3γ coincidence. The energy spectrum is also measured again. This time the main peak of the 2γ spectrum is cut off. Finally the hyper fine splitting and quenching is studied. For this the coincidence rate is measured for different applied magnetic field strengths.

4. Analysis

4.1. Delay setup

As has been explained in Section 3 the signals of the three single channel analyzers resulting from the same decay have to arrive at the coincidence unit at the same time in order for the unit to send out a logical yes to the linear gate to open it. To test this, the output signals of the SCAs are displayed with an oscilloscope. The signal of scintillator 2 is always used as trigger signal. The two compared scintillators are moved into the 180° configuration and the signals are averaged on the oscilloscope to obtain sharp signals. By comparing scintillator 2 with the two other signals and adjusting the delays at scintillator 1 and 3 the signals in Figure 5 are gained.

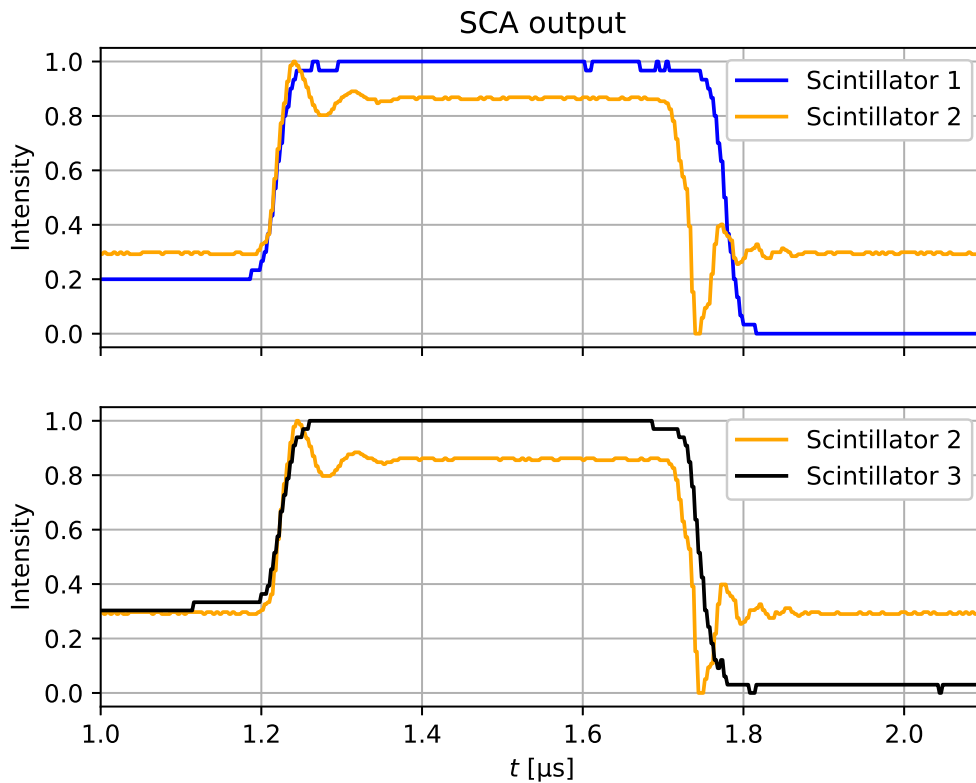


Fig. 5: Comparison of the signals of the single channel analyzers after the delays of scintillator 1 and 3 are set. Shown are signals from scintillator 1 (blue), scintillator 2 (orange) and scintillator 3 (black). The intensities are individually normalized. The input from scintillator 2 is used as trigger signal.

The delays are set so that always the rising flank of the signals are at the same time. As can be seen in Figure 5, the signals overlap nicely and therefore the chosen delay settings can be used in the following for the coincidence measurements.

4.2. ^{22}Na spectrum

The spectrum of the ^{22}Na source is measured with all three scintillators independently. Figure 6 shows the spectrum of scintillator 1. The other two are displayed in the appendix

in Figure 16 and 17.

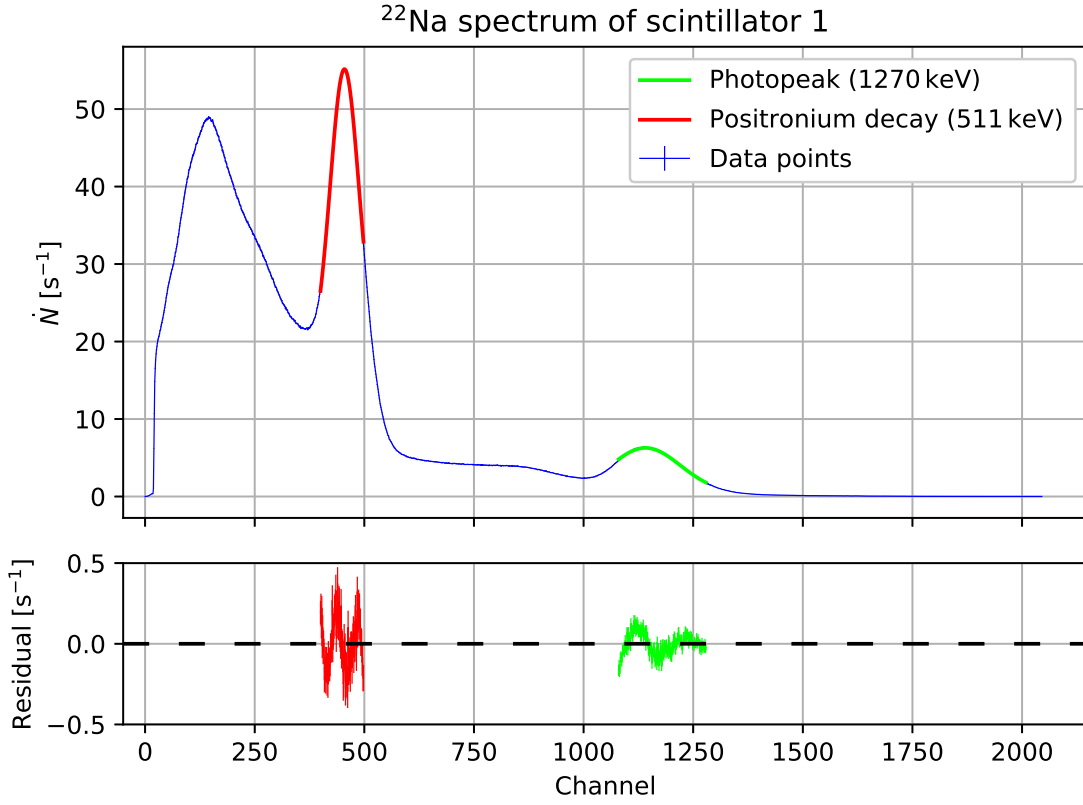


Fig. 6: Spectrum of ^{22}Na , measured with scintillator 1. Gaussian functions are fitted to the 1270 keV (lime) and 511 keV (red) peaks to acquire their channel positions. The small edges, which can be made out in front of the main peaks are the corresponding Compton edges. The lower picture shows the residuals of the fit functions with the data used for the fit.

To be able to identify channels with energies in all three scintillators, all three spectra are analyzed in the same way: The position of the peaks in the spectra, which originate from the decay of the ^{22}Na source at 1270 keV [1] and the 2γ decay of the positronium at 511 keV are determined. To determine the positions, Gaussian functions of the form

$$f(x) = \frac{A}{\sqrt{2\pi}\sigma} \exp\left\{-0.5\left(\frac{x-\mu}{\sigma}\right)^2\right\} + B \quad (4)$$

are fitted onto the data, where A is the reduced amplitude, B the offset, μ the expectation value and σ the standard deviation. Table 9 in the appendix lists the fit parameters for the three spectra.

Of these parameters the expectation values are used for the energy-channel calibration. Since the channels are discrete and the uncertainties on the expectation values are $s_\mu \ll 1$, the uncertainty on the channel number n is taken as $s_n = 1$.

In each spectra two channel numbers n_1 and n_2 and two corresponding energies $E_1 = 511$ keV and $E_2 = 1270$ keV are found. Equation 5, which is essentially a linear regression algorithm for two data points, is used to obtain the linear relation between energy and

channel number for each scintillator

$$E(n) = a \cdot n + b, \quad (5)$$

$$a = \frac{E_2 - E_1}{n_2 - n_1}, \quad (6)$$

$$b = E_1 - a \cdot n_1. \quad (7)$$

The parameters obtained for the three scintillators are listed in Table 1.

	scintillator 1	scintillator 2	scintillator 3
a [keV]	1.106 ± 0.002	0.912 ± 0.002	0.951 ± 0.002
b [keV]	8 ± 2	6.5 ± 1.3	6.4 ± 1.3

Tab. 1: Linear calibration parameters for Equation 5.

In the following Equation 5 will be used together with Table 1 to calculate energies from channels or to find appropriate channel windows for energies.

4.3. 2γ -coincidences

The measurements with 2γ -coincidences are used to characterize the setup. In the first section the random coincidences are analyzed. Then the angular dependence of the coincidences is studied. Finally the pressure dependence of the positronium production is observed.

4.3.1. Random coincidences

Using Equation 2 it is possible to calculate the random coincidence rate. Table 2 shows the measured counting rates of scintillator 1 and 2 obtained from a night measurement. For this, the two used scintillators are arranged, as described in the following Section 4.3.2.

	scintillator 1	scintillator 2
\dot{N} [s ⁻¹]	6064.4 ± 0.3	5815.5 ± 0.3

Tab. 2: Counting rates obtained in a night measurement with $T = 62\,454.22\text{ s}$ ($\approx 17.4\text{ h}$).

Using these rates and the time window $\tau_{\text{lit}} = 70\text{ ns}$ given in the instructions [8], one gets

$$\dot{N}_{\text{random}, 2\gamma}^{\tau_{\text{lit}}} = (4.9375 \pm 0.0003)\text{ s}^{-1}.$$

Additionally, by delaying one of the two signals it is possible to measure the random coincidence directly. For this a delay was put on scintillator 2. Table 3 shows the measured rates obtained after $T = 1000\text{ s}$.

	scintillator 1	scintillator 2	random coincidence
\dot{N} [s ⁻¹]	6080 ± 3	5835 ± 2	5.53 ± 0.07

Tab. 3: Random 2γ -coincidence rates obtained for $T = 1000\text{ s}$.

The big discrepancy of 8.5σ between the two random coincidence values could be explained with the given time window τ_{lit} from the instruction manual, for which no uncertainty is stated. From the measured data shown in Table 3 and Equation 2 rearranged, one can calculate

$$\tau_{\text{meas}} = (77.9 \pm 1.1) \text{ ns.}$$

This value deviates by 7.2σ from τ_{lit} . The uncertainty on τ_{meas} could be easily improved by means of a longer measurement time, but with a relative uncertainty of 1.4% its precision already suffices to discard the instructions value for τ .

Using τ_{meas} as the real value one can calculate the new value for the random 2γ -coincidences from the data obtained in the night measurement shown in Table 2

$$\dot{N}_{\text{random}, 2\gamma}^{\tau_{\text{meas}}} = (5.50 \pm 0.08) \text{ s}^{-1}.$$

To no surprise this coincides within less than 1σ with the directly measured value in Table 3. The uncertainty is dominated by the uncertainty from τ_{meas} .

However, the correctness of these considerations will be questioned and revoked in the context of the data from the random 3γ -coincidence measurement in Section 4.4.2.

In the following measurements, the rates are always corrected for with the directly measured random coincidence rate in Table 3, as it is the true value measured by the setup and does not depend on any calculations with assumed parameters.

4.3.2. Angular dependence

In order to find the best measurement position for 2γ -coincidences, scintillator 1 is moved in a range from 160° to 230° , while scintillator 3 is fixed at 260° . Figure 7 shows the resulting coincidences of scintillator 1 and 2, corrected by the random coincidence rate, as described in the previous section.

In order to determine the maximum counting rate, Equation 4 is fitted with the least square method onto the data, which is valid since the uncertainties on the angle have the same size. The corresponding fit parameters are listed in Table 4.

σ	μ	A	B	χ^2_ν
$(6.29 \pm 0.08)^\circ$	$(181.89 \pm 0.09)^\circ$	$(10\,914 \pm 162)^\circ \text{ s}^{-1}$	$(14 \pm 2) \text{ s}^{-1}$	7.5

Tab. 4: Fit parameters to the angular dependence of the counting rate. The function which is used to describe the data is Equation 4.

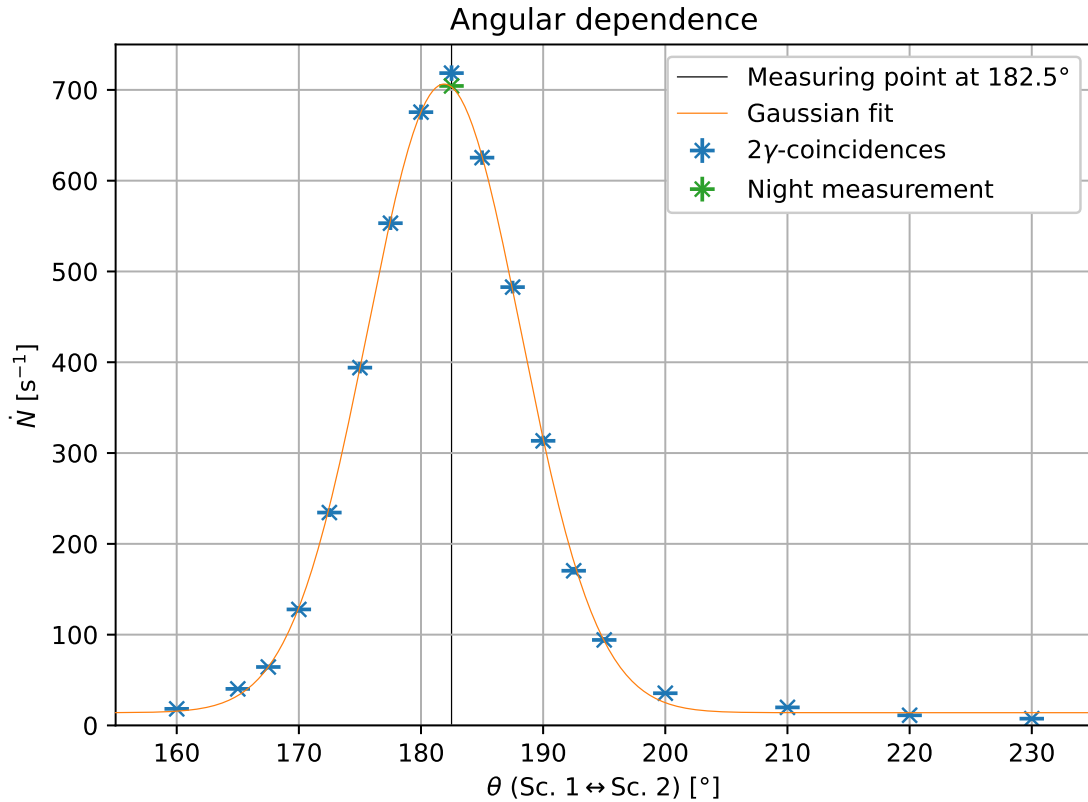


Fig. 7: Angle dependency of the coincidence rate between scintillator 1 and 2 (blue). The green data point is the result of an additional night measurement, which was performed over approximately 17 h. The orange function is a Gaussian fit to the data, not including the night measurement data, and the black line indicates the angle which is chosen for other 2γ coincidence measurements.

With this a maximum counting rate is found at $\theta = (181.89 \pm 0.09)^\circ$. Therefore the scintillator is set to the position marker closest to this angle, which is at 182.5° , indicated in Figure 7 as the black line. This is acceptable, since no significant difference in the rate is caused by this deviation. Furthermore, this setting allows to reproduce the results more easily. A smaller step width on the attached scale would allow a more precise positioning and also a more accurate determination of the maximum. The origin of the shift of around 2° away from the expected 180° is assumed to be the scale, which is glued to the setup and might be shifted from the exact position. Another possibility is that scintillator 2 is shifted relative to the setup. However, this seems unlikely, since the scintillator is screwed to the rest of the setup.

Since the maximum position is also used for further 2γ -coincidence measurements, the 182.5° position is measured more precise with an additional night measurement. The resulting counting rate coincides with the values expected from the fit function.

In Figure 8, the measured rates from the single scintillators in dependence of the relative angles are displayed.

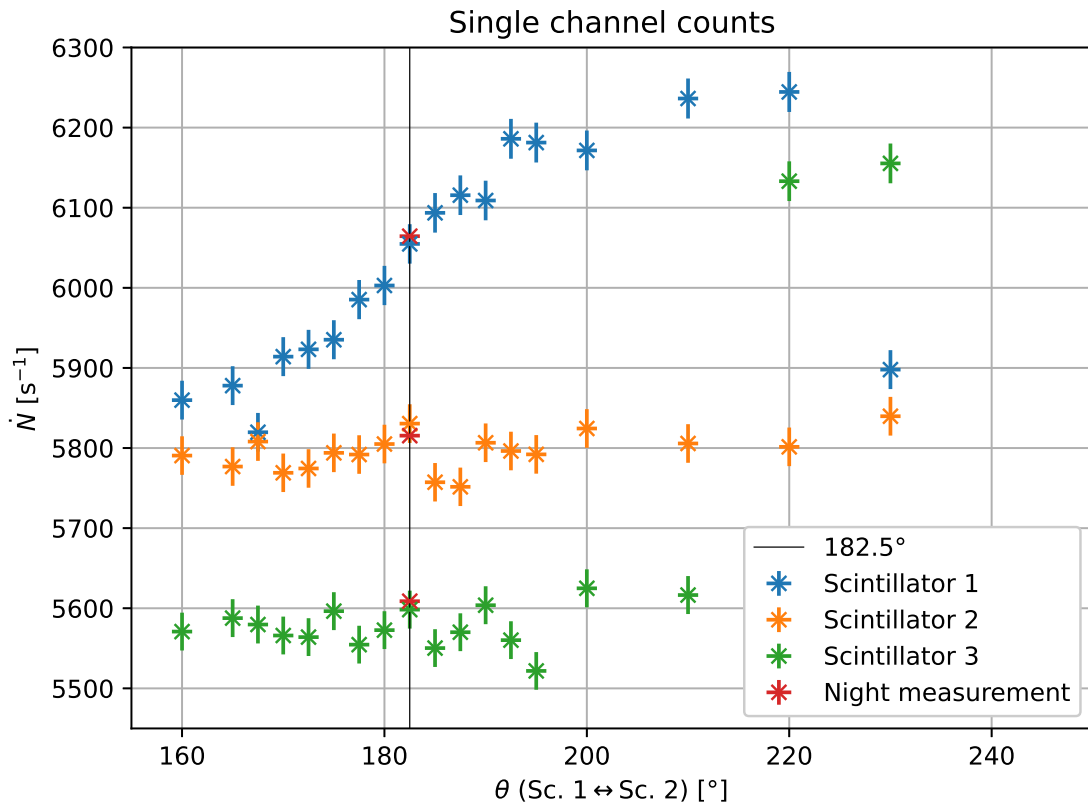


Fig. 8: Single counting rates of the angle measurement. The blue data is the signal of scintillator 1 the orange the one of scintillator 2 and the green one of scintillator 3. The angle at which the maximum coincidence counting rate is measured (see Figure 7), is indicated by the black line. Only the position of scintillator 1 is changed.

The rates of scintillator 2 and 3 show mostly a constant behaviour, which is also expected. Scintillator 1 on the other hand seems to have an increasing counting rate for bigger angles. The reason for this might be in the mounting of the radioactive source. It is, according to [8], fixed on a plastic film. The orientation and dimension of this film is not known. This might give some angle dependence to the single channel counting rate. The origin of the jumps in the counting rate of scintillator 1 and 3 at about 220° can not be analyzed here due to the few data points. For this some additional measurements in this range would be needed.

4.3.3. Pressure dependence

The amount of positronium depends on the pressure of the sulfur hexafluoride: With a higher pressure there are more electrons, which can be bound by the positron and thus form positronium, resulting in a higher counting rate. But also with a higher pressure the positron is slowed down faster, its probability to bind with an electron decreases. Because of this a maximum coincidence counting rate is expected at some pressure. Figure 9 shows the counting rates for pressures in the range of 0 bar to 7 bar of SF_6 , corrected by the random coincidences from Section 4.3.1. It can be seen that the counting rate increases up to 5.5 bar. Then a plateau is reached. The pressure chosen for the following measurements is 7 bar, to achieve maximal counting rates and therefore better statistics. The point at which the counting rate reduces again, could not be determined in this

experiment, since it was not possible to set pressures higher than 7 bar.

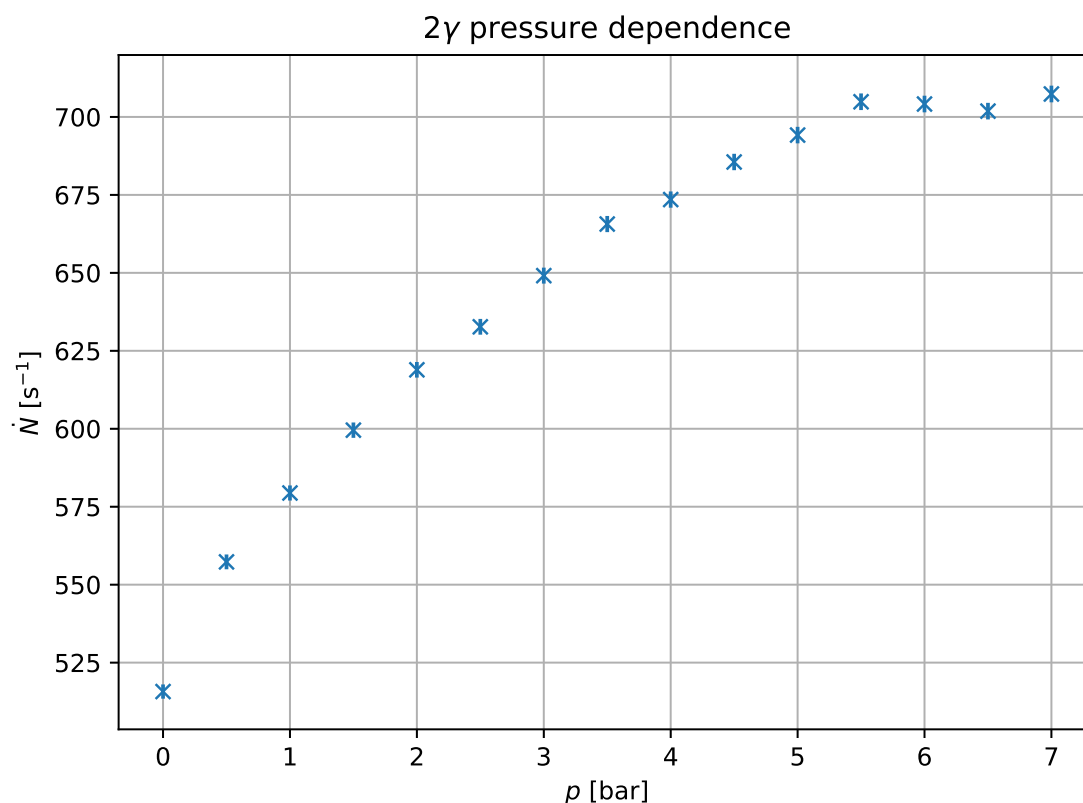


Fig. 9: Pressure dependence of the coincidence counting rate. The gas, of which the pressure is changed, is SF_6 . The coincidences are measured with the scintillators 1 and 2.

Figure 10 displays the individual counting rates of the two scintillators used for the coincidence measurement. Here the different behaviours of the counting rates attract attention. The counting rates measured by scintillator 1 rise with growing pressure, but the rates from scintillator 2 fall. Unfortunately, no explanation for this behavior has been found so far and further systematic investigations would have to be conducted. However, the expected behaviour of the coincidences in dependence of the pressure as shown in Figure 9, gives confidence in the correctness of the setup and the strange behaviour is ignored in the following measurements.

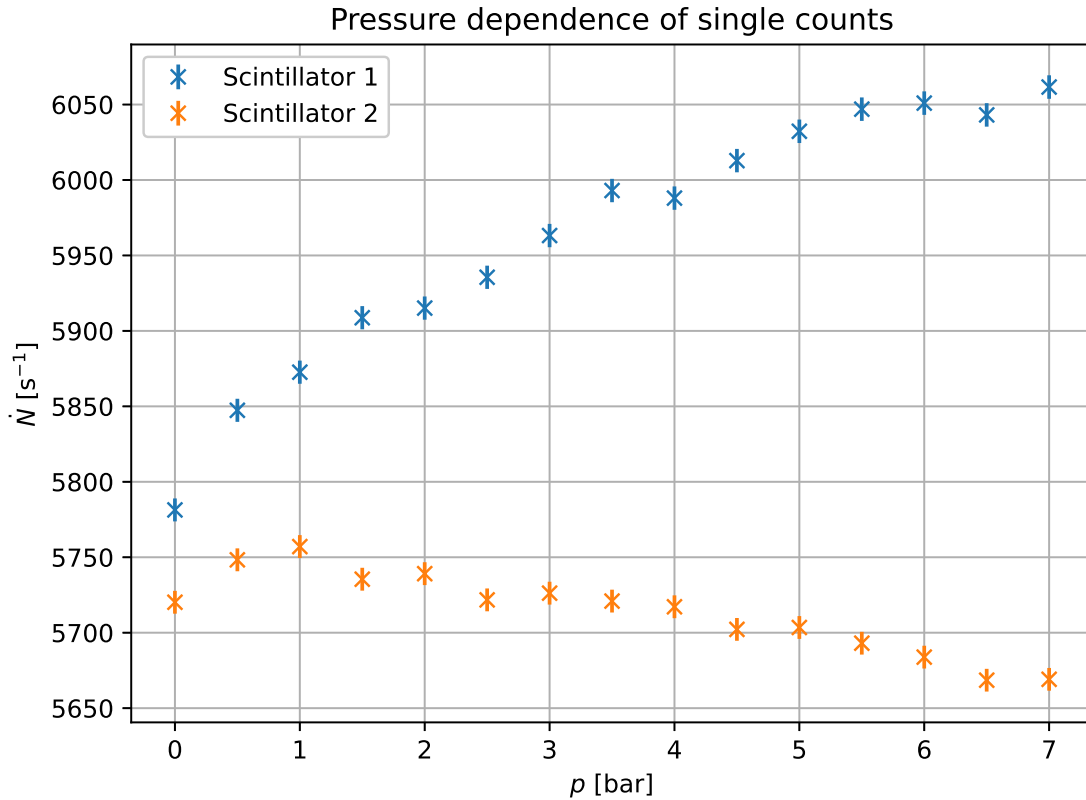


Fig. 10: Single counting rates of the scintillators 1 (blue) and 2 (orange), which are used to detect the coincidences at different pressures of SF_6 gas.

4.4. 3γ -coincidences

The setup is changed into a configuration where 3γ coincidences are measured with 180° between the three scintillators. This allows, after some preliminary measurements, the investigation of the quenching and the calculation of the hyper fine splitting. For this, also new background measurements are performed.

4.4.1. Energy spectrum

In order to measure the 3γ -energy spectrum the windows of the SCAs of scintillator 2 and 3 are set, so that they exclude the peak at 511 keV and all higher energies. The window of scintillator 1, which is connected to the computer, is fully open. The measurement time is approximately 25 h. This spectrum is shown in the appendix in Figure 13. The background, which is shown in Figure 14, is subtracted from the recorded spectrum and the corrected spectrum is displayed in Figure 15. In order to transform the channels into energy values the calibration from Table 1 for scintillator 1 is used. Figure 11 shows the resulting energy spectrum.

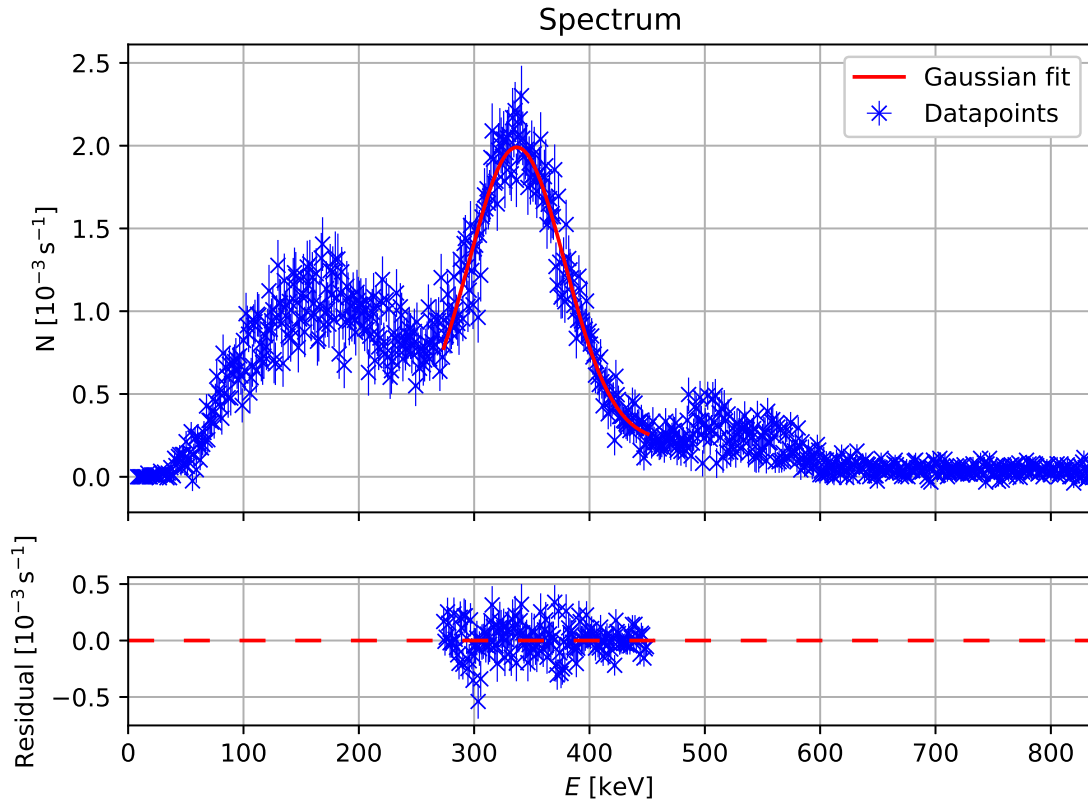


Fig. 11: Background reduced energy spectrum taken with scintillator 1 for the 3γ coincidences. The peak of the 511 keV is cut off by the SCAs of scintillator 2 and 3 so that the peak which is expected at around 340.7 keV is better seen. Onto this peak a Gaussian function is fitted. In the lower picture the residual of the Gaussian fit function is shown with the data used for the fit.

The main peak of the spectrum is fitted under the assumption of a normal distribution with Equation 4, in order to determine its position. Since the uncertainties on the energy are of similar size and small compared to the uncertainties of the rates, a least square fit including only the rate uncertainties is performed. The resulting fit parameters are listed in Table 5.

σ	μ	A	B	χ^2_ν
(41.8 ± 1.1) keV	(336.9 ± 0.6) keV	(185 ± 7) keV s $^{-1}$	(0.22 ± 0.03) s $^{-1}$	0.04

Tab. 5: Fit parameters of the Gaussian least square fit shown in Figure 11.

By taking again one channel as the uncertainty for the position of the peak, one gets

$$E_{3\gamma} = (337 \pm 9) \text{ keV.}$$

The theoretically expected value is one third of 1022 keV, the total energy of the positronium

$$E_{\text{theo}, 3\gamma} = 340.7 \text{ keV.}$$

Thus the experimentally measured energy is in good agreement with the theory, as it coincides within a 1σ interval with a relative uncertainty of 2.7%.

4.4.2. Random coincidences

As described in Section 4.3.1, the random 3γ -coincidence rate is calculated. The rates obtained from two night measurements (~ 30 h) are shown in Table 6.

	scintillator 1	scintillator 2	scintillator 3	random coincidence
\dot{N} [s^{-1}]	3663.4 ± 0.2	5901.0 ± 0.2	4606.2 ± 0.2	0.0098 ± 0.0003

Tab. 6: Counting rates obtained in two night measurements with $T = 107\,159.75$ s (≈ 30 h).

Using the measured scintillator rates displayed in Table 6, τ_{meas} from Section 4.3.1 and Equation 3 yields

$$\dot{N}_{\text{random}, 3\gamma}^{\tau_{\text{meas}}} = (1.81 \pm 0.05) \text{ ms}^{-1}.$$

This deviates strongly from the directly measured random coincidence rate, obtained with a delayed signal from one of the scintillators

$$\dot{N}_{\text{random}, 3\gamma}^{\text{meas}} = (9.8 \pm 0.3) \text{ ms}^{-1}.$$

Using $\tau_{\text{lit}} = 70$ ns from the instructions yields

$$\dot{N}_{\text{random}, 3\gamma}^{\tau_{\text{lit}}} = (1.463\,75 \pm 0.000\,11) \text{ ms}^{-1}.$$

Using the measured random coincidence rate and Equation 3 rearranged results in

$$\tau_{\text{meas}, 3\gamma} = (181 \pm 3) \text{ ns}.$$

This value deviates 34σ from the τ obtained from the random 2γ -coincidence measurement. This falsifies the considerations made earlier in Section 4.3.1. At this point a statement about the true value of τ cannot be made and the directly measured random coincidence counting rate is used for correcting the measured rates in the following.

Since the theory of Equation 2 and 3 is thoroughly tried and tested the cause of the deviations must lie in the used electronics or the used method to obtain the data. An uncertainty in the used method seems unlikely, since it is a standard method to utilize a delay to fully de-phase coincidences to obtain only random coincidences [18]. The used electronics are very old and have been used extensively over at least two decades and are therefore with high certainty the cause for the measured irregularities. However, this is not a problem, since the directly measured values accurately describe the behaviour of the used electronics. Only a time or temperature dependency of τ could cause deviations. In the following chapter the rates lie in the order of 0.10 s^{-1} . Since a variation of τ between 70 ns and 180 ns causes a difference of roughly 0.008 s^{-1} the effect would be small but not negligible. Two separate night measurements were performed for the random 3γ -coincidence rate. Evaluating both measurements individually yields

$$\tau_1 = (183 \pm 4) \text{ ns}, \quad \tau_2 = (179 \pm 4) \text{ ns}.$$

No significant deviation between the two values is found. For a definite statement about the time dependence of τ more measurements are required, but the collected data so far does not imply one.

4.4.3. Hyper fine splitting

In order to determine the splitting of the fine structure with 3γ decays, magnetic fields are applied. The fields are chosen in the range from 424 G to 6000 G. In order to determine the ratio between the counting rates with ($N(B)$) and without ($N(0)$) magnetic field. After three measurements with a magnetic field, $N(0)$ is determined again to compensate for any instabilities of the setup.

The ratio is expected to decrease for higher magnetic fields according to Equation 1, the theoretically derived formula for the quenching. There the factor f depends on the geometry of the setup. Since in this experiment the scintillators are set 120° apart, $f_{\text{theo}} = 0.5$ is expected [8]. The green line in Figure 12 shows the expected quenching function obtained from theoretical values which are listed in Section 2.2.

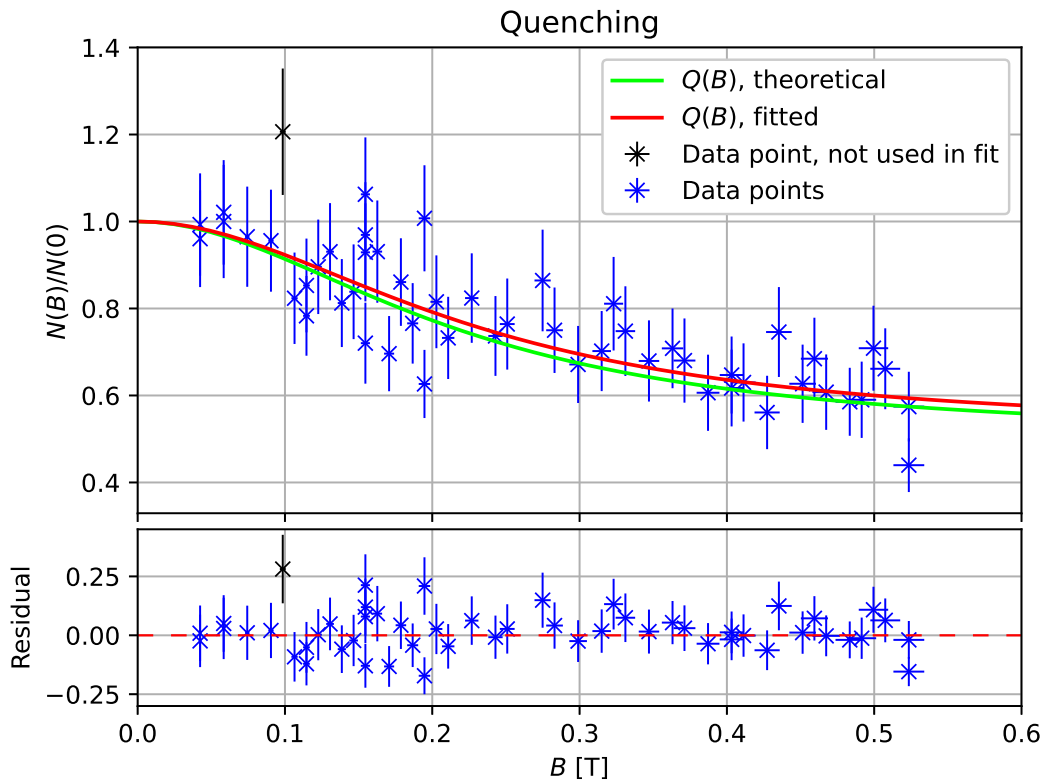


Fig. 12: The ratio between the counting number with and without magnetic field in dependence of the magnetic field is shown. The green line is the theoretically expected behaviour. The blue crosses are the measured data and the red line is the quenching function fitted to the data. The lower plot shows the residual of the fitted function. The black data point is not used for the fit, as it is an outlier.

Figure 12 also shows the experimentally measured data, corrected by the random coincidences from Section 4.4.2. Since $N(B)$ and $N(0)$ are measured for equal periods of time, in this part of the experiment N and not \dot{N} is considered. The same results would be obtained if \dot{N} would be used since the times cancel out. The uncertainties of $N(B)/N(0)$ are calculated with the assumption of Poisson distributed counts. The uncertainty on the magnetic field is 2%, according to [8].

The black data point at approximately 0.1 T is not used in the fit. It has to be an outlier,

since it is physically not reasonable to have a $N(B)/N(0) > 1$ under allowance of the uncertainty.

In order to determine the hyper fine splitting, Equation 1 is fitted to the data with the fit parameters f and ΔW . Since a least square fit is used, the uncertainties from the magnetic field are projected onto the y -axis with Equation 1, where the theoretical values for ΔW and f are inserted. These resulting uncertainties are then quadratically added to the count uncertainties. The resulting fit function, together with its residual, are shown in Figure 12. The fit parameters and the reduced χ^2 are listed in Table 7.

f	ΔW	χ^2_ν
0.49 ± 0.04	(215 ± 29) GHz	0.73

Tab. 7: Fit parameters for the quenching function in Figure 12.

The f -value indicates that three γ -quanta are detected since it is in a 1σ range to $f_{\text{theo}, 1} = 0.5$, with a relative uncertainty of 8.2%. Due to this, the fit is also performed with the f -factor fixed to 0.5 and results in a χ^2_ν of 0.74. This is shown in Figure 18 in the appendix. Here the resulting hyperfine splitting is $\Delta W_{f_{\text{theo}, 1}} = (225 \pm 13)$ GHz, which also is in a 1σ range to the fit with a free f .

An alternative value given by [8] is $f_{\text{theo}, 2} = 0.404$. This would indicate that only one γ is detected and the energies and angles of the other two are integrated over [8]. This is again used for an extra fit, which yields $\chi^2_\nu = 0.80$. The f -value measured with no preset f is in a 3σ range to $f_{\text{theo}, 2}$. Thus this interpretation of the setup does not fit very well to the result. The resulting hyperfine splitting is with $\Delta W_{f_{\text{theo}, 2}} = (164 \pm 13)$ GHz in a 2σ range to the result with a free f .

The hyper fine splitting of Table 7, holds a relative uncertainty of 13.5%. The experimentally measured value is in good agreement with the hyper fine splitting indicated in the literature $\Delta W_{f_{\text{theo}, 1}} = 204.4$ GHz [1].

The large uncertainty of ΔW might be a result of the deviations of the measured data from the function, especially in the range from 0.1 T to 0.2 T. In this area measurements were performed without turning off the power supply of the magnetic field after three measurements, which would have allowed the system to cool down. It is assumed that this has led to heating of the electronics and thus stronger deviating coincidence rates. It also might have resulted in differences between the current shown by the power supply and the one it actually provided, which causes a change in the applied magnetic field strength.

5. Summary and Discussion

The formation of different positronium states under the influence of a magnetic field was studied. For this preliminary characterizations and measurements were performed.

The spectrum of ^{22}Na is determined with all three scintillators. As expected, in each spectrum two main peaks are found, which correspond to the photon energy of 1270 keV of the ^{22}Na decay and 511 keV, which is the result of the 2γ decay of the positronium [1].

The random 2γ -coincidence background rate was experimentally determined, by delaying one scintillator signal, so that it can not coincide with the signal from the second scintillator caused by the same decay

$$\dot{N}_{\text{random}, 2\gamma} = (5.53 \pm 0.07) \text{ s}^{-1}.$$

This rate is used to correct the measured rates for 2γ -coincidence measurements.

In order to determine the angle correlation of the 2γ coincidence counting rate, the window of the SCA is set around the 511 keV peak. The angle between scintillator 1 and 2 is varied between 160° and 230° . It is found that the maximum counting rate is gained at

$$\theta = (181.89 \pm 0.09)^\circ.$$

Since this angle cannot be set with scale on the setup, the nearest mark at $(182.5 \pm 1.0)^\circ$ is chosen as the position for the scintillator. The deviation of the angle from 180° , which would be expected due to the momentum conservation of the 2γ decay, could have the following reasons: It can be a result of a shifted scale, or less probable, since it is screwed to the setup, a shift in the position of scintillator 2. Another origin of this shift might be the source. Since it is mounted on a foil of which neither size nor orientation are known, this also might have some influence on the maximum counting rate. By checking the counting rates of the single scintillators this assumption is substantiated. Here an angle dependence of scintillator 1, whose position is changed, is found. It is also found that scintillators, which are close together, seem to influence each other, as can be seen in Figure 8 for scintillator 1 and 3 at large angles. The mutual influence is no problem in this experiment, since the scintillators are 120° apart in the 3γ coincidence measurements and thus not in the critical region. What causes the influence could not be determined here. For this some additional tests would have to be performed.

To find the optimum gas pressure for which a maximum possible amount of positronium decays can be detected, the coincidence counting rate is measured for different pressures between 0 bar and 7 bar. Scintillators 1 and 2 are used for this. A plateau is found in the range of 5.5 bar to 7.0 bar. Because of this an operating pressure of 7.0 bar is chosen. The expected decrease of the counting rate at even higher pressures can not be observed due to the low pressure in the gas bottle, which limits the maximum pressure to 7 bar. The single counting rates of scintillators 1 and 2 in this measurement, show a behaviour which was not expected. One would expect both single counting rates to develop in similar ways. Instead the counting rate of scintillator 1 rises as expected for higher pressure, but that of scintillator 2 decreases slightly. No real explanation for this behaviour is found, especially since the coincidence rate increases. One possible source

of this behaviour might be that the counter for scintillator 2 is somehow broken, but in order to verify this assumption, scintillator 2 would have to be analyzed in more detail.

In order to measure 3γ coincidences, the SCA windows of scintillator 2 and 3 are closed so that the peak at 511 keV and higher energies are not measured. The three scintillators are positioned with 120° between them. At first, the spectrum, which is gathered with scintillator 1, is measured together with a background spectrum, which is subtracted from the main spectrum. To get the energy spectrum, the calibration, which was done with the peaks of the ^{22}Na -spectrum, is used. In this way the energy of the 3γ decay is determined to be

$$E_{3\gamma} = (337 \pm 9) \text{ keV}.$$

This is in a 1σ range to the theoretically expected value of $E_{\text{theo}, 3\gamma} = 340.7 \text{ keV}$ with a relative uncertainty of 2.6 %.

The random 3γ -coincidence background rate is also obtained by delaying one of the signals and results in

$$\dot{N}_{\text{random}, 3\gamma} = (9.8 \pm 0.3) \text{ ms}^{-1}.$$

Finally, the hyperfine splitting of positronium is determined by measuring the 3γ coincidences with different magnetic fields applied. By fitting Equation 1 to the data the fine splitting

$$\Delta W_{f_{\text{free}}} = (215 \pm 29) \text{ GHz}$$

with a relative uncertainty of 13.5 % and the f -value

$$f_{\text{free}} = 0.49 \pm 0.04$$

are found. This is compared to the splitting which is obtained for the two f -values $f_{\text{theo}, 1} = 0.5$ and $f_{\text{theo}, 2} = 0.404$, proposed by [8]. For both values of f the splitting is determined and listed in Table 8.

f_{theo}	$\Delta W[\text{GHz}]$
0.5	225 ± 13
0.404	164 ± 13

Tab. 8: Hyper fine splitting results which are determined with fixed f -values.

The free f -value is in a 1σ range to $f_{\text{theo}, 1}$ and 3σ to $f_{\text{theo}, 2}$ with a relative uncertainty of 8.2 %. This indicates that the fitted value is in better agreement with $f_{\text{theo}, 1}$, but due to the relative uncertainty also a description by $f_{\text{theo}, 2}$ would be possible.

The splitting $\Delta W_{f_{\text{free}}}$ is also better described by $\Delta W_{f_{\text{theo}, 1}}$, to which it is in a range of less than 1σ , whereas $\Delta W_{f_{\text{theo}, 2}}$ deviates by 3σ . It follows that $f_{\text{theo}, 1}$ seems to describe this experiment better, which is expected due to the geometry of the setup.

Comparing $\Delta W_{f_{\text{free}}}$ to the literature value $\Delta W_{f_{\text{lit}, 1}} = 204.4 \text{ GHz}$ [1], which was used in the plot in Figure 12, a deviation of less than 1σ is found. This is also the case, if the result of a precision measurement of the ground state hyperfine splitting is considered [2],

where $\Delta W_{\text{lit}, 2} = (203.3942 \pm 0.0016)$ GHz was determined.

The large uncertainty on ΔW , which relativizes the good agreement with the literature, is assumed to origin mainly from the scattering of the counting rates in the measurements between 0.1 T and 0.2 T. This might be due to the heating of the coils, since those measurements were performed with no brake in between, where the power supply for the B -field would be turned off. Also the $\chi^2_{\nu} < 1$ indicate, that noise is present in the data, and the algorithm is overfitting the data.

Appendix

A. Error propagation

If the N variables x_i of a function f are not correlated,

$$s_f = \sqrt{\left(\frac{df}{dx_1} s_1\right)^2 + \dots + \left(\frac{df}{dx_N} s_N\right)^2} \quad (8)$$

is used with the error s_i of x_i . In case that the variables are correlated,

$$s_f = \sqrt{(\nabla f)^T \cdot M \cdot \nabla f} \quad (9)$$

has to be applied. Here M is the covariance matrix.

B. Additional Plots

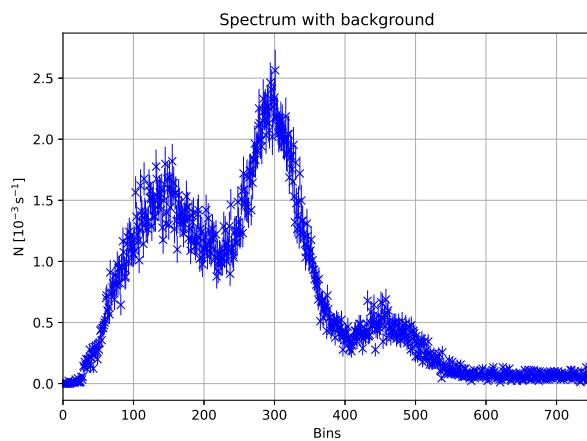


Fig. 13: Spectrum of the 3γ -coincidence measurement without subtracted background.

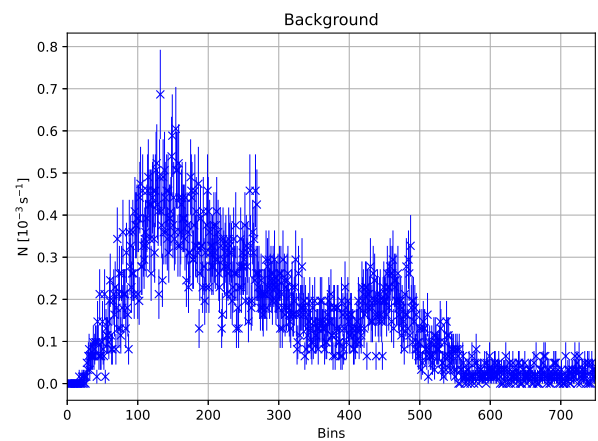


Fig. 14: Background of the 3γ -coincidence measurement.

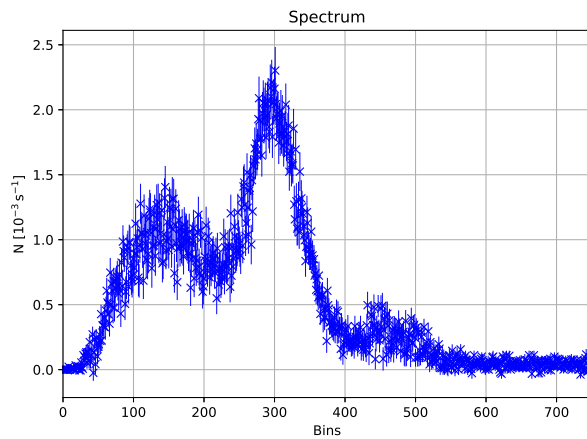


Fig. 15: 3γ -spectrum with background subtracted.

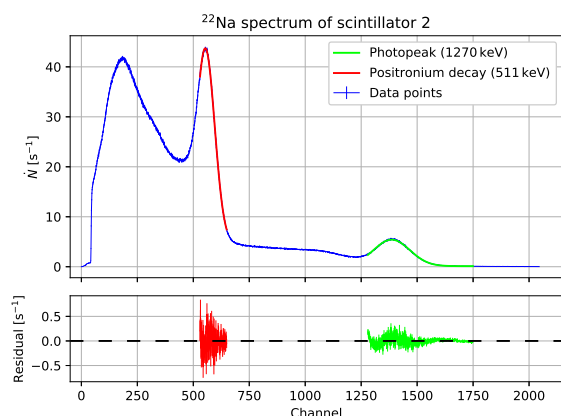


Fig. 16: ^{22}Na spectrum measured with scintillator 2. Gaussian functions are fitted to the 1270 keV (lime) and 511 keV (red) peaks to acquire their channel positions. The small edges, which can be made out in front of the main peaks are the corresponding Compton edges. The lower picture shows the residuals of the fit functions with the data used for the fit.

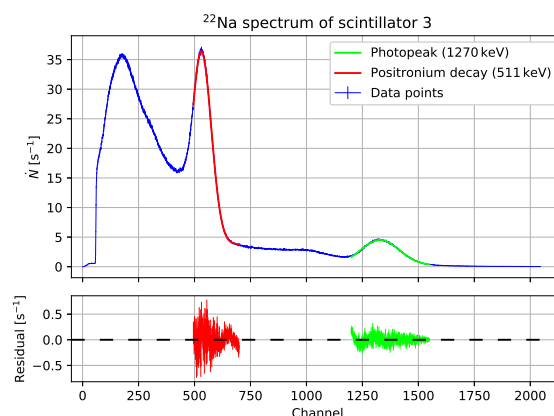


Fig. 17: ^{22}Na spectrum measured with scintillator 3. Gaussian functions are fitted to the 1270 keV (lime) and 511 keV (red) peaks to acquire their channel positions. The small edges, which can be made out in front of the main peaks are the corresponding Compton edges. The lower picture shows the residuals of the fit functions with the data used for the fit.

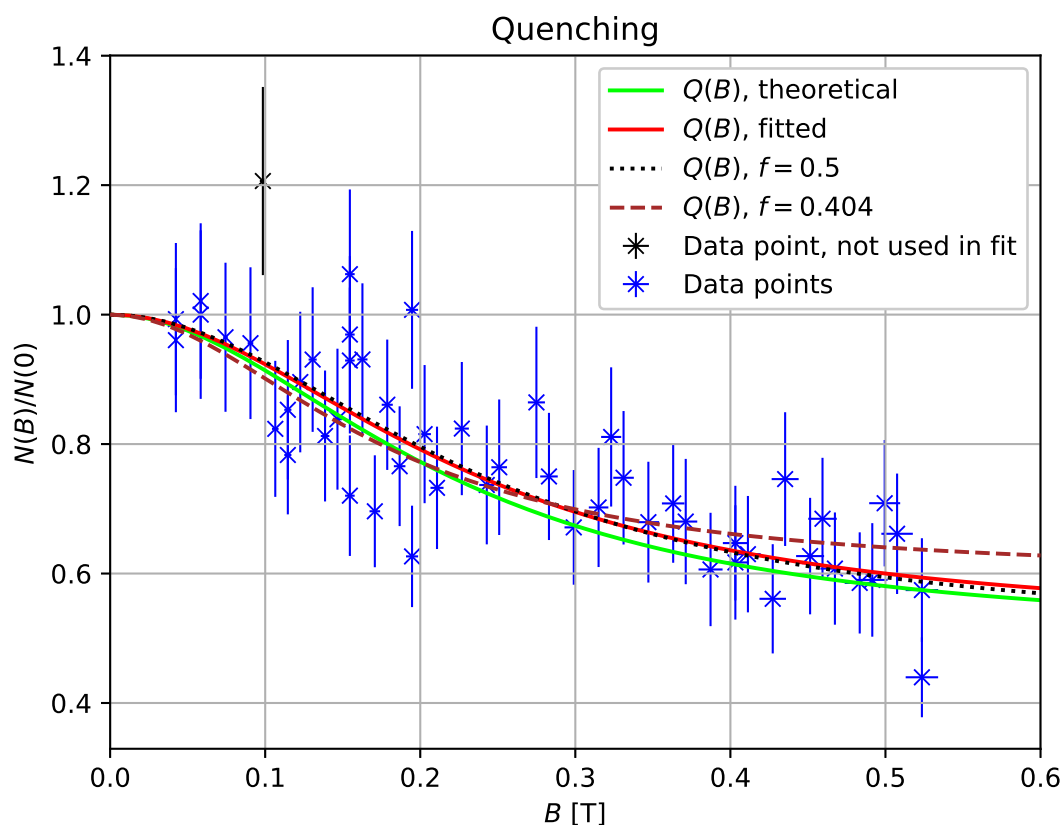


Fig. 18: Quenching measurement with additional fit functions where the geometry factor is set to $f = 0.5$ (black dotted) and $f = 0.404$ (brown). The other functions are as in Figure 12.

C. Additional Tables

	scintillator 1		scintillator 2		scintillator 3	
	positronium	photopeak	positronium	photopeak	positronium	photopeak
μ	454.70 ± 0.03	1141.1 ± 0.2	553.49 ± 0.10	1386.2 ± 0.2	530.47 ± 0.09	1328.5 ± 0.2
σ	32.4 ± 0.2	79.8 ± 0.7	42.05 ± 0.14	81.1 ± 0.2	44.23 ± 0.08	86.2 ± 0.3
A [s ⁻¹]	3062 ± 34	1151 ± 18	4134 ± 20	1078 ± 2	3619 ± 7	930 ± 4
B [s ⁻¹]	17.5 ± 0.2	0.52 ± 0.05	4.48 ± 0.07	0.120 ± 0.002	3.790 ± 0.014	0.217 ± 0.009
χ^2_ν	2.9	3.9	1.1	2.0	1.4	1.5

Tab. 9: Fit parameters to the energy spectra which are shown in Figure 6, Figure 16 and Figure 17.

D. List of Figures

1.	First order Feynman diagrams of the decay of positronium into 2 and 3 γ 's.	5
2.	Energy ranges of interaction processes of photons with matter.	6
3.	Schematic setup.	10
4.	Setup of the electronic components.	11
5.	Comparison SCA signals.	13
6.	Spectrum of ^{22}Na taken with scintillator 1.	14
7.	Angle dependency between scintillator 1 and 2.	17
8.	Single counting rates of the angle measurement.	18
9.	Pressure dependence of the coincidence counting rate.	19
10.	Rates of scintillators 1 and 2 at different pressures.	20
11.	Energy spectrum for the 3γ coincidences.	21
12.	Quenching of the counting rate in dependence of the B -field.	23
13.	Spectrum of the 3γ -coincidence measurement.	28
14.	Background of the 3γ -coincidence measurement.	28
15.	3γ -spectrum with background subtracted.	28
16.	^{22}Na spectrum measured with scintillator 2.	29
17.	^{22}Na spectrum measured with scintillator 3.	29

E. List of Tables

1.	Linear calibration parameters for Equation 5.	15
2.	Random 2γ -coincidence night measurement rates.	15
3.	Random coincidence rates.	15
4.	Fit parameters to the angular dependence of the counting rate.	16
5.	Fit parameters of the Gaussian least square fit shown in Figure 11.	21
6.	Random 3γ -coincidence night measurement counting rates.	22
7.	Fit parameters for the quenching function in Figure 12.	24
8.	Hyper fine splitting results which are determined with fixed f -values.	26
9.	Fit parameters to the energy spectra.	30

F. References

- [1] BÜNDGE, VOLKER. *Magnetisches Quenching des Positroniums*, 1975.
- [2] A. ISHIDA et al. *New precision measurement of hyperfine splitting of positronium*. Physics Letters B, 734:338–344, 2014.
- [3] MOHOROVIČIĆ, S. *Möglichkeit neuer Elemente und ihre Bedeutung für die Astrophysik*. Astronomische Nachrichten, 253 (4): 93–108, 1934.
- [4] DEUTSCH, MARTIN. *Evidence for the formation of positronium in gases*. Physical Review, 82 (3): 455, 1951.
- [5] KARSHENBOIM, SAVELY. *Precision study of positronium: Testing bound state QED theory*. International Journal of Modern Physics A, 19 (23): 3879–3896, 2004.

- [6] JONES, BILLY, et al. *Analytic treatment of positronium spin splittings in light-front QED*. Physical Review D, 55 (10): 6561, 1997.
- [7] BASS, STEVEN. *QED and fundamental symmetries in positronium decays*. arXiv preprint <https://arxiv.org/abs/1902.01355>, 2019.
- [8] KASCHEK, D. & KÖHLI, M. *Positronium - Advanced Experimental Practice II*, 2009/2011.
- [9] MESCHEDE, DIETER. *Gerthsen physik*. Springer-Verlag, 2015.
- [10] LANGHOFF, H. *Die Feinstruktur des Positroniums*. Physik in unserer Zeit, 2: 44–47, 1976.
- [11] LOHMANN, ERICH. *Hochenergiephysik*. Teubner Stuttgart, 1981.
- [12] HAKEN, HERMANN & WOLF, HANS CHRISTOPH. *Atom-und Quantenphysik: Einführung in die experimentellen und theoretischen Grundlagen*. Springer-Verlag, 2000.
- [13] PRATT, R. H. *Tutorial on fundamentals of radiation physics:: interactions of photons with matter*. Radiation Physics and Chemistry.
- [14] NELSON, G., et al. *Gamma-Ray Interactions with Matter*. <https://faculty.washington.edu/agarcia3/phys575/Week2/Gamma%20ray%20interactions.pdf>. Accessed: 2020-09-17.
- [15] EINSTEIN, ALBERT. *Über einm die Erzeugung und Verwandlung des Lichtes betreffenden heuristischen Gesichtspunkt*. Annalen der Physik, 4, 1905.
- [16] COMPTON, ARTHUR. *A quantum theory of the scattering of X-rays by light elements*. Physical review, 21 (5): 483, 1923.
- [17] LEO, WILLIAM. *Techniques for Nuclear and Particle Physics Experiments - A How-to Approach - 2nd Edition*. page 118, 1994.
- [18] LEO, WILLIAM. *Techniques for Nuclear and Particle Physics Experiments - A How-to Approach - 2nd Edition*. 1994.

G. Acknowledgements

We thank our Tutor Florian Hasse for his support in the experiment.

H. Laboratory Journal

Positronium

28.07.2020

Day 1

1. ^{22}Na -Spectrum measurement

Using the NaI_1 scintillator, the Σ windows of the SCT wide open and with the computer software GammaVision the spectrum is measured.

↳ NA_spec_1 .TKA ← first number live time [s]
second number ~~real~~ real time [s]

↳ measurement duration 5005 seconds

↳ ~~Preliminary~~ preliminary evaluation: looks as expected

^{22}Na -source is from the year 31.12.2004. Activity then: $3.81 \cdot 10^6 \text{ Bq}$
Half-life time 2.602 years ~~to~~

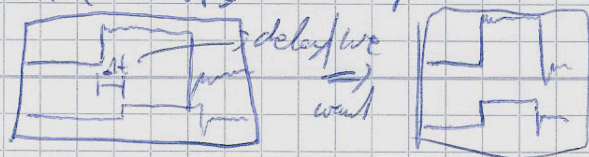
2. The Correlation of 2γ -decay

Now we check, if any additional delays ~~between~~ for the signals of the individual ~~to~~ scintis are needed.

We use the $2\gamma^+$ -decay, because we ~~then~~ can discriminate the ~~signal~~ ~~of~~ signals to only register the 511 keV ~~peaks~~ ~~peaks~~.

We then compare the signals from Scinti 2 (red) with Scinti 3 (blue) and then the signal from Scinti 2 with ~~to~~ Scinti 1 (yellow).

To do so, we take the signals after the SCT's and input them into the oscilloscope. →



Discrimination windows SCA's

We set the windows on each SCA to only show the 511 keV peak.

Scinti 3 (blue, channel C @ coincidence unit):

spectrum after window is set \rightarrow scinti3_window.TKA
position
~~angle~~: 182.5°

Scinti 1 (yellow, channel A @ coincidence unit):

position: 182.5°

spectrum \rightarrow scinti-1_window.TKA

Scinti 2 (red, channel B @ coincidence unit):

fixed position (0°)

spectrum \rightarrow scinti-2_window.TKA

Delay check

First, we compare Scinti 2 with Scinti 1: \rightarrow at 182.5°

after some adjustments with the delay ~~off~~ for Scinti 1

\hookrightarrow delay_2=1.csv (Channel 1: Scinti 1, 100mV div)
(Channel 2: Scinti 2, 2V div)
(Time: 200ns div)

Now Scinti 2 with Scinti 3: \rightarrow at 182.5°

after some minor adjustments

\hookrightarrow delay_2_3.csv (Channel 2: Scinti 2, 2V div)
(Channel 3: Scinti 3, 50mV div)
(Time: 200ns div)

2. Angle Correlation @ 2γ -decay

We now measure the angle correlation @ the 2γ -decay (para-positronium).

To do so, we use scinti 1 and 2. 2's position is fixed, the angle between 1 and 2 is changed by moving 1 around.

The angle is indicated by ~~an~~ a scale that is glued to the setup, with division up to 2.5° (near only near the 180° mark).

Scinti 3 is at position $\approx 260^\circ$, so its ~~data~~ data is also measured ≈ 10 s (but not coincidence relevant), to ~~to~~ hopefully see no change (with changing position of scinti 1).

We measure at each set angle for 100 seconds, and write down the counts of each scinti and the coincidence count of scinti 1 and 2.

Angle	Scinti 1	Scinti 2	Scinti 3	Coincidence
150°				
160°				
165°				
167.5°				
170°				
172.5°				
175°				
177.5°				
180°				
182.5°				
185°				
187.5°				
190°				

$\pm 1^\circ$ strange angle dependency

Angle	Scinti 1	2	3	Coincidence
150°	58 0 537	58299	56070	175
160°	58598	57906	55709	238
165°	58779	57769	55877	458
167.5°	58197	58081	55797	699
170°	59141	57691	55660	1333
172.5°	59232	57745	55640	2400
175°	59352	57940	55964	3996
177.5°	598 8 53	57919	55546	5587
180°	60029	58050	55727	6810
182.5°	60548	58305	55983	7240
185°	60936	57573	55503	6309
187.5°	61156	57516	55701	4883
190°	61090	58066	56038	3190
192.5°	61860	57963	55602	1759
195°	61913	57921	55278	997
200°	61715	58244	56249	410
210°	62363	58057	56765	254
230°	58979	58397	61553	130
220°	62445	58015	61331	167

Measurement over night - 2x coincidence

Scinti 1 at 182.5°

Day 2

29.07.2020

→ results from ~~the~~ overnight-measurement

Scinti 1: 378749310

Scinti 2: 363200644

3: 350294082

Coincidence: 44333615

Time: 6245422/100 seconds

3. Random Coincidence

Looking at the angle correlation measurement from the day before, we find a strange angle dependency on the counting rate from scint. 1.

~~For the following background~~

Maybe we will look into this ~~at~~ more detailed at some later ~~of~~ time, but for now we just take it as it is and ~~to~~ ~~test~~ ~~leave~~ position scint. 1 at the 182.5° position for the background measurements.

Initially, we ~~to~~ wanted to shift it to some other angle to achieve ~~and~~ only random coincidences, but this strange angle dependency ~~that~~ makes us not do this.

Therefore we only ~~shift~~ ^{use} the delays ~~to~~, so that no real coincidence will be measured.

We ~~shift~~ ~~the~~ ~~delay~~ ^{change} the delay ~~of~~ on Scint. 2 from the 0.1-1.1 ns ~~setting~~ to the 1-11 ns setting.

Instantly we see the rate ~~on~~ the coincidence count drop. We ~~now~~ ^{now} measure for 1000 seconds.

From the instructions we know $N_{\text{random}, 2p} = 2 \cdot N_1 \cdot N_2 \cdot \tau$

Which is wrong...
[Counts] \neq [s] \downarrow

with τ the coincidence time window. The instruction manual says

$\tau = 70 \text{ ns}$. ~~With this and N_1, N_2 we~~

$$N_{\text{random}, 2p} = 2 \cdot N_1 \cdot N_2 \cdot \tau \quad \rightarrow \quad \frac{N_{\text{random}, 2p}}{\tau} = 2 \cdot \frac{N_1}{\tau} \cdot \frac{N_2}{\tau} \cdot \tau$$

$$\Rightarrow \boxed{N_{\text{random}, 2p} = 2 \cdot N_1 \cdot N_2 \cdot \frac{\tau}{T}}$$

~~The~~ $T = 1000 \text{ s}$, $N_{\text{random}, 2p} = 5530$

$N_1 = 629680$ 6079680

$N_2 = 5834860$

$N_3 = 6127526$ (@ 270°)

} preliminary with $\tau = 70 \text{ ns}$
 $\rightarrow N_{\text{random}, 2p} = 4966$

With this we can calculate τ

$$\rightarrow \tau = \frac{N_{\text{random}, 2\gamma} T}{2 \cdot N_1 \cdot N_2} \stackrel{\text{preliminary}}{\approx} 77.94 \text{ ns}$$

\rightarrow We will repeat this measurement again to get more data/precise

After some discussion, we now measure N_1 and N_2 for 100s with no delay applied. We should yield the same results (withing uncertainty as before).

$$N_{\text{coinc}} = 711167$$

$$N_1 = 6088419$$

$$N_2 = 5836519$$

$$N_3 = 6427086$$

$$T = 100 \text{ s}$$

preliminary

\rightarrow

$$\text{with } \tau = 70 \text{ ns} \rightarrow N_{\text{coinc}} \approx 4974$$

~~random~~
random

\rightarrow To calculate τ we need to use ~~the~~ ~~the~~ delay, to truly ~~the~~ only get random coincidences.

4. Pressure dependency @ 2γ -coincidence

$$T = 100 \text{ s},$$

pressure (bar)	N_{cosine}	N_1	N_2
0	52125	578137	572018
0.5	56284	584738	574831
1	58493	587264	575708
1.5	60508	590874	573545
2	62444	591512	573913
2.5	63823	593553	572176
3	65464	596319	572621
3.5	67118	599302	572095
4	67903	598800	571719
4.5	69108	601285	570220
5	69971	603228	570346
5.5	71040	604894	569305
6	70967	603095	568382
6.5	70739	604313	566853
7	71239	606160	566911
7.5			
8			

↳ Can't set higher pressure

@ ~ 5 bar ~~substantially~~ it saturates.

In the following measurements we use 7 bar as pressure.

2 γ -coincidence @ 7 bar

$$T = 323429/100 \text{ seconds}$$

$$\text{@ } 112.5^\circ \quad N_1 = 19605294, N_2 = 18344572, N_3 = 19884420 \quad \text{@ } 270^\circ$$

$$N_{\text{coinc}} = 2309231$$

5. 120° - 3 γ -coincidence ~~spe~~ energy spectrum

Scinti 2 ~~and~~ and 3 have upper limit close to 5M channel,
Scinti 1 detects full range.

120°-configuration, 3 γ -coincidence

- first test measurement $T = 291625/100$ seconds

$$N_1 = 45724910 \quad N_3 = 35564290$$

$$N_2 = 45181344 \quad N_{\text{coinc}, 3\gamma} = 1639$$

Spectrum file \rightarrow scinti_1_3-coinci.TK1

\hookrightarrow real time: ~~2918~~ 2915.3715

~~live~~ live time: 2915.367s

\Rightarrow interesting: scinti 3 ~~had~~ has 10 million fewer counts
than scinti 1 and 2.

~~Reason~~ Reason unclear. ~~Be~~

For now we ~~conclude~~ say, ~~that~~ that it is probably just a ~~diff~~
different amplification level. This only results in a fewer
coincidences, but ~~doesn't~~ ^{shouldn't} affect the spectrum measurement.

We ignore this for now, and compare with the measurements.
Maybe we ~~to~~ will have time ~~at~~ later to study this
phenomenon.

~~We set up~~

We now repeat the same measurement with a ~~much~~ a much larger time scale. We aim ~~for~~ for ~~~~~ 25 hours, followed by ~16 hours background measurement (using delays).

30.07.2020

Day 3

Collecting the ~25 hour 3γ -coincidence-energy-spectrum data:

$N_1 = 1227964377$, $N_2 = 1148098942$, $N_3 = 880241638$
 $N_{\text{coinc}} = 50760$, $T = 9013019/100$ seconds

energy spectrum file \rightarrow 3_gamma_coinci_Energy_spec.TKA

Real time: 90112,323s

Live time: 90112,203s

\rightarrow 25.03 hours measurement time

Now we put a delay on scinti 2, to get random coincidences.

We also measure the energy spectrum, to get ~~the~~ ^{the} background for ~~the~~ ^{the} in the spectrum.

This will run ~16.5 hours.

Day 4

31.07.2020

We now collect the data from the background measurement and do a quick preliminary evaluation.

$N_1 = 832610159$, $N_2 = 777966408$, $N_3 = 596521115$
 $N_{\text{coinc}} = 8368$, $T = 6119536/100$ seconds

See Spectrum from Scinti 1

↳ file: 3_gamma_coinc-Energy-back.TKA

Real time: 61173,987s

Live time: 61173,967s

We ~~can~~ now ~~se~~ normalize the data to 1 second, to be able to subtract the background from the data.

• We unplugged all 3 Scintis, and checked, whether the electronics ~~is~~ noise is strong enough to generate counts.

↳ 28 min.
After $T = 167393/100$ seconds no counts are detected.

$N_1 = N_2 = N_3 = N_{\text{coinc}} = 0$

6. Magnetic Quenching

We use the spectrum measurement to determine ~~the~~ the channels we want to use for the 340 keV-line.

→ ~~220~~ 220-400 channel range

Now we input each scinti into the PC ~~to~~ (no coincidence), to set the windows on the SCTs to the channel range.

~~Files~~ We use no coincidence to get data fast. We will only see the normal ^{22}Na -spectrum, but we know from the ~~spectra~~ ^{22}Na -spectrum measurement, which channels we want to use.

Scinti 1 \rightarrow 3_gamma_scinti_1_windows.TKA

Scinti 2 \rightarrow - " - - 2 - " -

Scinti 3 \rightarrow - " - - 3 - " -

~~We look~~ After we set up the windows we looked at

the spectrum of Scinti 2 for \sim 9 minutes and concluded from that data, that our procedure for setting the windows

only works for Scinti 1. \rightarrow File 3_gamma_scinti_3 ~~File~~ Energy_spec.TKA

Since ~~as~~ each Scinti has a different amplification level, we would need a calibration measurement for each Scinti to ~~identify channels with energy~~. convert channel number to energy.

\Rightarrow From our energy spectrum measurement, we know ^{at} which energy range the 340 keV peak is placed.

$$\Rightarrow \boxed{254 \text{ keV} - 57470 \text{ keV}}$$

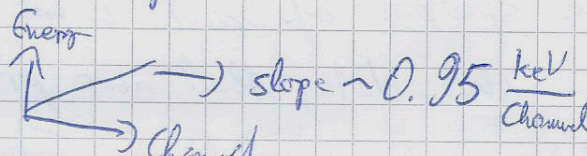
We now measure the ^{22}Na -spectrum for Scinti 2 and 3 to get a energy-channel-calibrations.

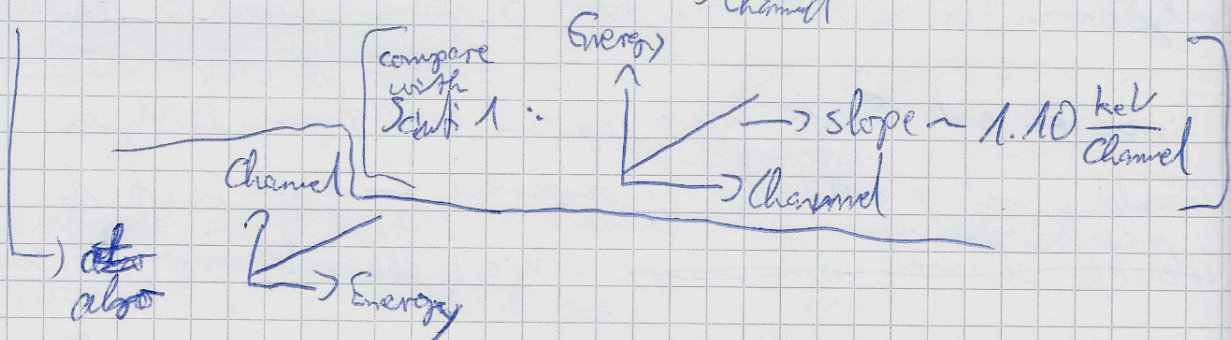
$$\begin{aligned} N_1 &= 654546, N_2 = 611394, N_3 = 200446, & (3\gamma\text{-coinci}) \\ N_{\text{coinci}} &= 498, T = 534052/100 \text{ seconds} \end{aligned}$$

Scinti 3 Σ ^{22}Na -Spectrum \rightarrow File Na_Spec_3.TKA

$N_1 = 2595646$, $N_2 = 3976222$, $N_3 = 12452338$
 $N_{\text{coinci}} = 12446910$, $T = 74331/100$ seconds
 (only coinci with Scinti 3)

Scinti 2 ^{22}Na -Spectrum \rightarrow File Na_Spec_2.TKA

\rightarrow preliminary evaluation Scinti 3:  slope $\sim 0.95 \frac{\text{keV}}{\text{Channel}}$

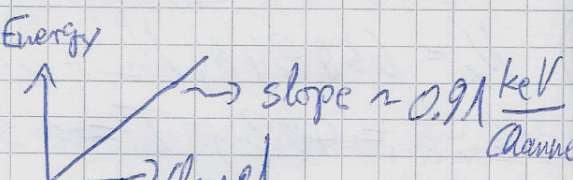


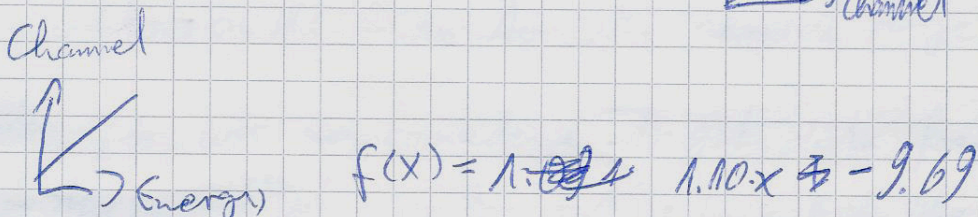
$$f(x) \approx 1.06 \cdot x - 14.59$$

\Rightarrow ~~Energy range~~ Channel Range for Scinti 3: $\boxed{253 - 482}$

Scinti 2 ^{22}Na -Spectrum \rightarrow File Na_Spec_2.TKA

$N_1 = 3200254$, $N_2 = 19271452$, $N_3 = 15356699$
 $N_{\text{coinci}} = 19271441$, $T = 91647/100$ seconds ~ 15 min
 (only from Scinti 2)

\rightarrow preliminary evaluation: Scinti 2:  slope $\sim 0.91 \frac{\text{keV}}{\text{Channel}}$



\rightarrow Channel Range for Scinti 2: $\boxed{269 - 506}$

We set the windows accordingly, and measure the $\beta\gamma$ -coincidence spectra for each Scinti, to ~~check~~ check the signal.

Spectrum from Scinti 3 \rightarrow 3_gamma-sciinti_3_Energy_spec_new.TKA

$$N_1 = 22401940, N_2 = 38871078, N_3 = 30436063$$
$$N_{\text{coinc}} = 936, T = 641534/100 \text{ seconds}$$

Now a quick $B=0$ $\beta\gamma$ -coinc
 $I = 0.03 \text{ A}$

~~$N_1 \rightarrow$ ~~TKA~~ ~~TKA~~~~

$$N_1 = 3490871, N_2$$

$$N_1 = 3490871, N_2 = 6063317, N_3 = 4746554,$$
$$N_{\text{coinc}} = 155, T = 100000/100 \text{ seconds}$$

Spectrum for $I_B = 0, 03 \text{ A} \rightarrow$ B_003A_S21.TKA

Spectrum for $I_B = (7.01 \pm 0.01) \text{ A} \rightarrow$ ~~B_701A~~ B_701A_S71.TKA

$$N_1 = 3396613, N_2 = 5924599, N_3 = 4606466$$
$$N_{\text{coinc}} = 107, T = 100000/100 \text{ seconds}$$

Spectrum for $I_B = 15.00 \text{ A}$ ~~at~~ ~~at~~ after 1000s $I_B = 14.47 \text{ A}$
 \rightarrow Not stable at all!

\rightarrow File B_1500A_S71.TKA

$$N_1 = 3342726, N_2 = 5982041, N_3 = 4483480$$
$$N_{\text{coinc}} = 82, T = 100000/100 \text{ seconds}$$

03.08.2020

Day 5

Collecting the data for the 3 γ -coinci-energy spectrum,
with ~~the~~ Scinti 2 ~~set~~ and 3 ~~set~~ set to the channels
The windows of
obtained from before. Scinti 1 is wide open.

#

This measurement ran over the weekend.

File \rightarrow 3_gamma-coinci-energy-spec-new.TKA

$N_1 = 3109982303$, $N_2 = 1379830615$, $N_3 = 1077711488$
 $N_{\text{coinci}} = 60010$, $T = 22919208/100$ Seconds
 \hookrightarrow 2nd - 64 hours.

We set the windows on Scinti 1 to the range 254 keV - 470 keV ago
 \hookrightarrow File 3_gamma-scinti1-new.TKA

6. Averaging

$T = 1000$ s

I [A]	N_{coinci}	N_1	N_2	N_3
0.03	143	3690053	5970840	4678973
1.00	143 142	3687191	5977727	4674463
1.40	146	3686159	5976072	4679686
1.80	138	3680424	5970496	4668109
0.03	136	3694381	5992514	4686496
2.20	130	3679930	5971421	4660581
2.60	112	3669347	5956943	4651132
2.80	116	3669825	5954807	4646528

Continue next page

T = 10005

I [A]	Meas	N_1	N_2	N_3
0.03	144	3695266	5984857	4680321
3.00	129	3665529	5957004	4645079
3.20	734	3658376	5943696	4634709
3.40	117	3658428	5937622	4631208
0.03	130	3687573	5982877	4681642
3.60	109	3652935	5930679	4622788
3.80	126	3647663	5927732	4622407
4.00	121	3646583	5919125	4615528
0.03	158	3686174	5980315	4677288
4.20	110	3642891	5911865	4612213
4.40	136	3636995	5905050	4607101
4.60	121	3631456	5901031	4602232
0.03	136	3687089	5980669	4678773
4.81	137	3631399	5895072	4599680
10.01	88	3558766	5802101	4510580
7.00	102	3596279	5846923	4555056

Random Coinc - 3gamma - Night measurement

Day 6

04.08.2020

$N_1 = 188498388$, $N_2 = 305546642$, $N_3 = 238893563$

Meas = 528, T = 5129016/100 seconds.

3γ - random coincidence. Delay on Sent 2 (like the 2γ - random-coinc. measurement)

T=1000s

I [A]	N _{crine}	N _A	N _B	N _C
0.03	166	3671255	5945336	4652747
4.80	104	3613350	5860497	4578442
13.03(12)	73	3526545	5775044	4439047
2.80	130	3648430	5907430	4624372
0.03	126	3669084	5944454	4652771
11.22(2)	79	3535712	5771408	4471670
2.40	152			
2.40	152			
→ Temperature dependency?				
↳ 20 min - amp # off				
↳ 0.03	142	3669837	5944938	4654315
↳ lunch break, and amp off!				
0.03	152	3672635	5950602	4655399
12.03(13)	89	3534441	5775538	4460394
1.00	146	3668035	5945513	4648119
6.00	112	3601908	5847572	4546292
↳ Amp off	148	3675190	5955634	4656067
0.03	128	3674083	5951812	4655795
8.00	152			
3.80	136			
10.02(2)	79	3548548	5787196	4487077
3.80	136	3633171	5894589	4601848
0.03	141	3671601	5952013	4654116
3.80	131	3635748	5897199	4598237
7.80	99	3572498	5803289	4515080
13.02	81	3519712	5763242	4446910

Day 7

06.08.2020

All the ~~the~~ equipment was turned off for one day, since the buildings ~~power~~ power was turned off for maintenance.

T=1000s

I [A]	N_{coins}	N_1	N_2	N_3
0.03	144	3633183	5787725	4584412
9.02	102	3526339	5658396	4444271
5.20 power of current off	102			
0.03	142	3648042	5840601	4620079
3.20	104	3587439	5765046	4533908
5.60	117	3583172	5772778	4529890
0.03	123	3648619	5858450	4625070
10.60	69	3529104	5686043	4450746
1.20	84	3577196	5754362	4526957
8.20	92	3553779	5714190	4489480
0.03	122	3652982	5856217	4627074
11.20	72	3520277	5678771	4434425
11.20	72			
0.03	122	3660697	5861266	4634691
9.20	83	3545534	5710209	4478742
8.60	103	3547425	5707093	4488958

07.08.2020

Day 8

Night measurement, 3-g random coincidence.

~~#~~ $N_1 = 204070603$, $N_2 = 326803114$, $N_3 = 254700749$,
 $N_{\text{coinci}} = 522$, $T = 5586959/100$ seconds

↳ ~ 15.4 hours

~~hours: Hex scaler with no input~~

Hex scaler input with no inputs, counted $N = 4$.

~~A(A)~~ to do $I(A)$: ~~3.80, 5.60, 6.80, 7.40, 8.60, 9.60, 1.40, 8~~

~~0.03~~
~~3.80~~
~~5.60~~

$T = 1000_s$

$I(A)$	N_{coinci}	N_1	N_2	N_3
0.03	131	3711759	594843	4711549
8.60	89	3540341	5692251	4475720
1.40				
0.03	118	3646629	5835452	4621877
1.40	118	3640450	5831202	4605165
6.80	102	3560707	5720245	4504311
0.03	127	3647903	5837080	4625949
9.60	77	3465151	5678267	4465151
8.00	103	3549629	5706623	4495540
0.03	143	3651467	5846874	4627914
7.40	96	3558751	5717717	4507997
3.80	103	3614797	5785596	4580482

$$T = 1000 \text{ s}$$

$I (A)$	N_{count}	N_1	N_2	N_3
0.03	130	3649142	5847623	4633703
5.00	106	3599916	5763871	4559957
11.60	79	3522312	5679574	4451387
11.40	89	3529324	5681442	45 4453981
0.03	122	3651435	58851236	4647728
10.80	91	3533212	4467830	5687966
6.00 0.03	1000 127	3859782	5857575	4646318
12.63	84	3526701	5687368	4441716
12.40	90	3527730	5681068	4449490
10.20	180	3539775	5691963	4539775